

# Institutionen för systemteknik

## Department of Electrical Engineering

**Examensarbete**

## **Validation and Improvement of MVEM in HIL Simulator**

Examensarbete utfört i Fordonssystem  
vid Tekniska högskolan vid Linköpings universitet  
av

**Jesper Sandberg**

LiTH-ISY-EX--12/4574--SE

Linköping 2012



**Linköpings universitet**  
**TEKNISKA HÖGSKOLAN**



# Validation and Improvement of MVEM in HIL Simulator

Master's thesis  
performed in **Vehicular Systems**  
**Dept. of Electrical Engineering**  
at **Linköping University**

**Jesper Sandberg**

LiTH-ISY-EX--12/4574--SE


Supervisors: **Ph.D. Student Andreas Thomasson**  
ISY, Linköping University  
**M.Sc. Per Östli**  
SCANIA CV AB, System Test Engine  
**M.Sc. Andreas Bolin**  
SCANIA CV AB, System Test Engine  
**B.Sc. Marcus Johansson**  
SCANIA CV AB, System Test Engine

Examiner: **Associate Professor Lars Eriksson**  
ISY, Linköping University

Linköping, 20 June, 2012





	<b>Avdelning, Institution</b> Division, Department  Division of Vehicular Systems Department of Electrical Engineering Linköpings universitet SE-581 83 Linköping, Sweden	<b>Datum</b> Date  2012-06-20
<b>Språk</b> Language  <input type="checkbox"/> Svenska/Swedish <input checked="" type="checkbox"/> Engelska/English  <input type="checkbox"/> _____	<b>Rapporttyp</b> Report category  <input type="checkbox"/> Licentiatavhandling <input checked="" type="checkbox"/> Examensarbete <input type="checkbox"/> C-uppsats <input type="checkbox"/> D-uppsats <input type="checkbox"/> Övrig rapport <input type="checkbox"/> _____	<b>ISBN</b> _____ <b>ISRN</b> LiTH-isy-ex--12/4574--se <b>Serietitel och serienummer ISSN</b> Title of series, numbering _____
<b>URL för elektronisk version</b>  <a href="http://www.control.isy.liu.se">http://www.control.isy.liu.se</a> <a href="http://www.ep.liu.se">http://www.ep.liu.se</a>		
<b>Titel</b> Title Validering och Förbättring av Motormodell i HIL Simulator Validation and Improvement of MVEM in HIL Simulator  <b>Författare</b> Jesper Sandberg Author		
<b>Sammanfattning</b> Abstract  <p>In this master's thesis, a validation method for engine models in a HIL simulator is developed. To make the validation automatic, a script has been written in the programming language Python that executes the engine model in the same way as the real engine in a test cell at Scania CV. Variables in the model are recorded in real-time and compared to recordings from the engine test cell. The validation method handles static as well as dynamic engine model validation. The submodels in the current engine model that causes the most deviation from engine test cell data are identified. One of them, i.e. the turbine model, is improved by creating a semi-physical model of a Variable Geometry Turbine (VGT). Furthermore, future improvements have been suggested.</p>		
<b>Nyckelord</b> Keywords MVEM, ECU, HIL, Validation, Turbocharging, Modeling		



# Abstract

In this master's thesis, a validation method for engine models in a HIL simulator is developed. To make the validation automatic, a script has been written in the programming language Python that executes the engine model in the same way as the real engine in a test cell at Scania CV. Variables in the model are recorded in real-time and compared to recordings from the engine test cell. The validation method handles static as well as dynamic engine model validation. The submodels in the current engine model that causes the most deviation from engine test cell data are identified. One of them, i.e. the turbine model, is improved by creating a semi-physical model of a Variable Geometry Turbine (VGT). Furthermore, future improvements have been suggested.



# Acknowledgments

I would like to thank the members of System Test Engine at Scania CV and especially my supervisors; Per Östli for great knowledge about engine models, Marcus Johansson for advanced programming skills and Andreas Bolin for valuable experience from engine test cells. Together, we have developed a validation method that will be useful for Scania CV in the future. I also send special thanks to my examiner Lars Eriksson and my supervisor Andreas Thomasson at Vehicular Systems. Your support and interesting ideas have guided me in the right directions during the thesis.

Finally, I would like to thank my girlfriend Anna. You make every day special.

Jesper Sandberg



# Contents

<b>1</b>	<b>Introduction</b>	<b>1</b>
1.1	Background . . . . .	1
1.2	Purpose . . . . .	1
1.3	Goals . . . . .	1
1.4	Resources . . . . .	3
1.5	Delimitations . . . . .	3
1.6	Related work . . . . .	3
<b>2</b>	<b>Approach</b>	<b>5</b>
2.1	Scania DC13 Engine . . . . .	5
<b>3</b>	<b>HIL simulator</b>	<b>9</b>
3.1	HIL Simulation . . . . .	9
3.2	dSpace HIL Simulator at Scania . . . . .	9
3.2.1	ControlDesk . . . . .	10
3.2.2	Mean Value Engine Model . . . . .	11
<b>4</b>	<b>Validation</b>	<b>15</b>
4.1	Background . . . . .	15
4.1.1	Dynamometer . . . . .	15
4.1.2	PID controller . . . . .	15
4.2	Steady state validation . . . . .	18
4.2.1	Test data . . . . .	18
4.2.2	Validation with controlled VGT and EGR positions . . . .	20
4.2.3	Validation by controlling the intake flow with the VGT position	24
4.2.4	Validation of compressor and turbine model . . . . .	30
4.3	Transient validation . . . . .	32
<b>5</b>	<b>Turbocharging</b>	<b>35</b>
5.1	Turbine performance . . . . .	35
5.1.1	Turbine map . . . . .	37
5.2	Compressor performance . . . . .	37
5.2.1	Compressor map . . . . .	38
5.3	Turbo Dynamics . . . . .	38

<b>6</b>	<b>Modeling</b>	<b>39</b>
6.1	Existing turbine model . . . . .	39
6.2	Turbine model . . . . .	39
6.2.1	Turbine mass flow . . . . .	40
6.2.2	Turbine efficiency . . . . .	41
6.2.3	Parametrization . . . . .	42
6.2.4	Validation . . . . .	42
<b>7</b>	<b>Future work</b>	<b>45</b>
<b>8</b>	<b>Summary and conclusions</b>	<b>47</b>
8.1	Summary . . . . .	47
8.2	Conclusions . . . . .	47
	<b>Bibliography</b>	<b>49</b>
<b>A</b>	<b>Simulink models below the top layer</b>	<b>51</b>
<b>B</b>	<b>Figures from static validation with VGT and EGR control</b>	<b>56</b>
<b>C</b>	<b>Figures from static validation with control of compressor flow and EGR position</b>	<b>59</b>
<b>D</b>	<b>Figures from dynamic validation</b>	<b>63</b>



# Chapter 1

## Introduction

### 1.1 Background

The Engine Management System (EMS) is an Electric Control Unit (ECU) that controls the engine in modern trucks. The software in this control unit continuously increases in size and complexity. To ensure that the EMS meets the high requirements, testing is an important part. At Scania CV these tests are performed in trucks but also in so called Hardware-In-the-Loop (HIL) simulators. Within these simulators the control unit is connected with the same I/O as in a vehicle. The difference from ECU testing in a vehicle is that the environment of the control unit, for example engine, gearbox and aftertreatment system, is simulated with mathematical models that runs in real-time. The outputs from the ECU are then connected to the model so that a closed loop system is created.

### 1.2 Purpose

The purpose of this thesis is to increase the confidence of the automated EMS testing at Scania, by validation and improvement of a mathematical engine model.

### 1.3 Goals

To be able to improve the current engine model in the HIL simulator, this model has to be validated against data from an engine test cell. The first goal of this thesis is therefore to develop a method for engine model validation against engine test cell data. The method should be implemented as a Python-script to be run as an automated test of engine performance in the HIL simulator. It should be applicable to static as well as dynamic engine model validation. The purpose of the validation method is to find the weak parts of the current engine model. The second goal is to improve the part of the model that causes the most deviation from engine test cell data.

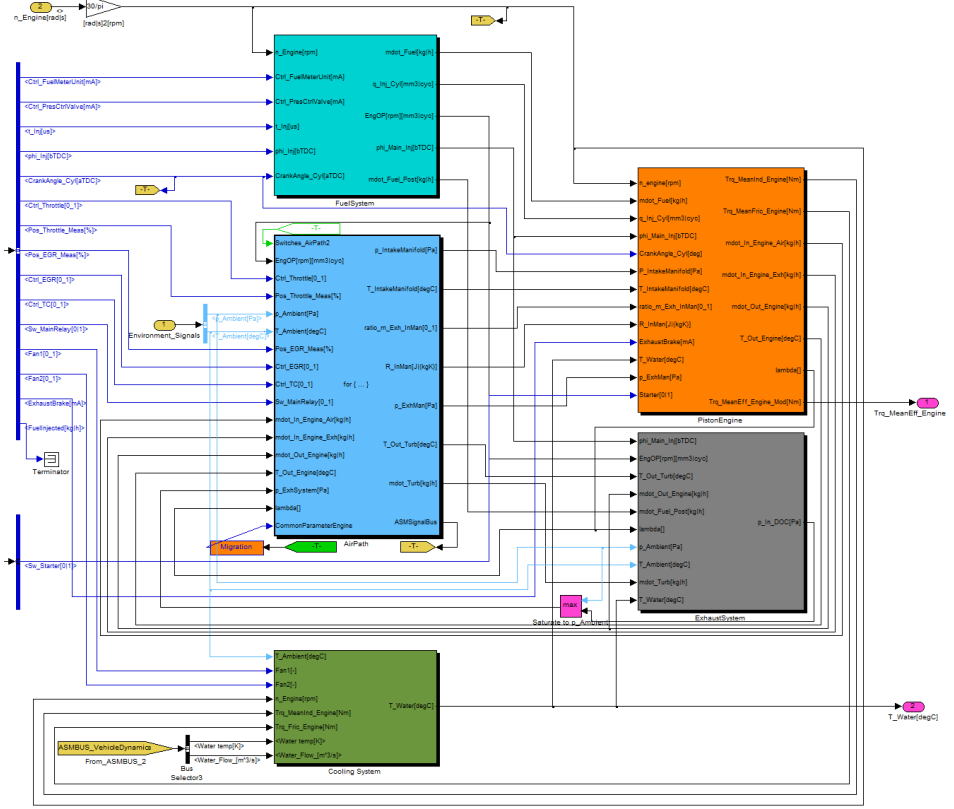


**Figure 1.1.** Overview of the engine model in the HIL simulator. The block *FuelSystem* controls the fuel flow to the engine. *AirPath* describes the mass flows, pressures and temperatures in the engine. *PistonEngine* calculates the induced torque. *ExhaustSystem* describes the aftertreatment system and *CoolingSystem* models the engine cooling system. The content of each block can be found in Appendix A on page 51.

## 1.4 Resources

HIL simulator at Scania CV. Mathematical model of a Scania DC13 engine, see figure 1.1 on page 2, created by dSpace in Matlab Simulink. Test automation framework developed by Scania in the programming language Python to communicate with the HIL simulator. Static as well as dynamic data recordings from engine test cell.

## 1.5 Delimitations

This thesis will focus on validation and improvement of an engine model with corresponding aftertreatment system. The rest of the driveline (clutch, gearbox, retarder etc.) will not be included in the validation. The static as well as the dynamic behaviour of the model will be studied, but the different control algorithms of the engine will be ignored.

## 1.6 Related work

A lot of studies has been done on mean value engine modeling. Basic engine theory is described in [7] along with an introduction to mean value engine modeling. In [11], mean value models and several control systems are discussed thoroughly. A complete mean value engine model with Variable Geometry Turbine (VGT) and Exhaust Gas Recirculation (EGR) is developed in [15] and [16]. The model is statically as well as dynamically validated using measurements from an engine laboratory at Scania CV. In [8], an engine model is developed with a strategy to find a submodel for each engine component. The resulting model is validated on a Saab 2.3 litre production engine. A modeling methodology that focuses on the gas and energy flows in engines is described in [9]. The methodology is applied on a EGR/VGT equipped diesel engine. In [6], a complete MVEM is implemented in Matlab Simulink. The article also discusses turbo maps and turbo modeling thoroughly. Exhaust system temperatures are discussed in [5].

Validation of engine models are included in most of the literature that discusses mean value engine modeling. In [2], several different mean value models are validated. A brief review of HIL simulation is given in [12]. Simulations and tests in a HIL simulator are discussed in [1], [4] and [13]. In [14], a whole HIL system is developed and used as a testbench for an ESP unit. The information about the HIL simulator at Scania is collected from [3] and basic control theory can be found in [10].



# Chapter 2

## Approach

In this thesis, an automated validation method has been developed in order to compare measurements from an engine model in a HIL simulator against data from a real engine in a test cell. Since the inputs to the engine model are controlled in real-time by the EMS, the validation in this thesis is a lot more complicated than model validation in general. Therefore, a lot of work has been done to make the comparison reliable. The HIL simulator is controlled by an automated test script, written in the programming language Python. Variables in the model are recorded in real-time and validated against static as well as dynamic measurements from an engine test cell at Scania CV. The validation method is applicable to other engine models than the one used in this thesis, to facilitate the future model validation process at Scania. To validate an existing model in the HIL simulator with the validation method developed in this thesis, only sensor data from an engine test cell is required.

### 2.1 Scania DC13 Engine

The current engine model, developed in Matlab Simulink, is shown in figure 1.1 on page 2. The model is a complete Mean Value Engine Model (MVEM) of a Scania DC13 engine. The MVEM approach is intended to capture dynamics over one or more cylinder cycles. The sub-cycle dynamics are not modeled, therefore the model computational speed is high.

Scania DC13, figure 2.2, is a Compression Ignited (CI) diesel engine with a piston displacement of 12.7 litres. The maximum power is 480 hp at the engine speed 1900 rpm. Maximum torque is 2500 Nm, between 1000 and 1300 rpm. This engine complies to the Euro VI emission requirement. It is equipped with Variable Geometry Turbine (VGT), Exhaust Gas Recirculation (EGR) and Selective Catalytic Reduction (SCR). VGT is used to control the compressor flow by adjusting the effective area in the turbine. With EGR, the hot exhaust gases are cooled in the EGR cooler and then recirculated to the intake manifold (figure 2.1). This leads to a smaller amount of nitrogen oxides ( $NO_x$ ) out from the engine, since this gas

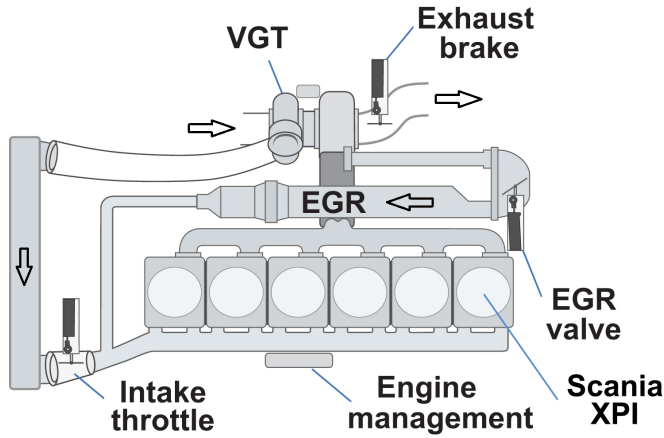


**Figure 2.1.** Schematic view of a Scania DC13 engine, equipped with VGT and EGR. The airflow in the engine is shown by the arrows. The intake air flows through the compressor and intercooler (leftmost in the figure) and is then mixed with the exhaust gases from the EGR. After the combustion process, the hot exhaust gases flow through the turbine, which is used to drive the compressor.

is produced at high temperatures. SCR is an emission technology with the aim to reduce the  $NO_x$  emissions by converting these gases into diatomic nitrogen ( $N_2$ ) and water ( $H_2O$ ).

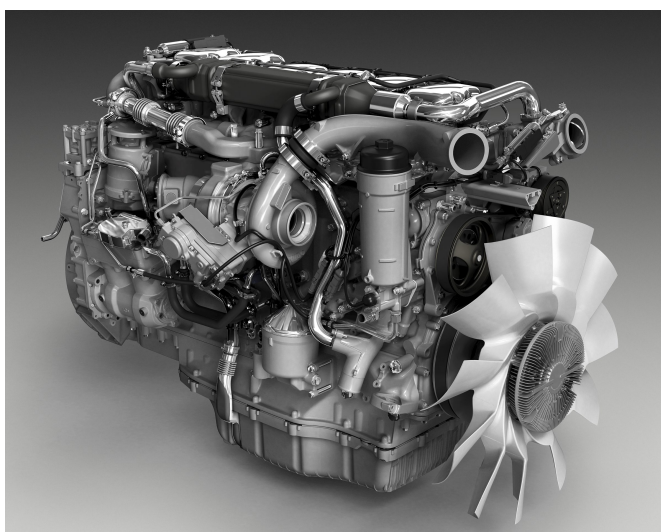


**Figure 2.2.** *Scania DC13 engine. 6 cylinders, total piston displacement of 12.7 litres.*





# Chapter 3

## HIL simulator

### 3.1 HIL Simulation

The tight development schedules in the automotive industry do not allow the design and testing of embedded systems to wait for an available prototype. Therefore, Hardware-In-the-Loop (HIL) applications are used by design and test engineers to evaluate and validate vehicle components during development of new control systems, assemblies and vehicles. Instead of testing these components in complete system setups, HIL simulation makes it possible to test new components and prototypes while communicating with software models that simulate the rest of the system.

For the development and test of Electric Control Units, ECU:s, this means that the rest of the vehicle is replaced by computers running software models. The ECU being tested responds to the simulated signals as though it was operating in a real vehicle. This is due to that the control unit cannot distinguish between the signals sent by other physical components and signals provided by software models running on a computer. A HIL simulator can handle test drives outside the range of what a real vehicle can do, and the tests are reproducible and automatable. These simulations also increases the opportunity to try out dangerous test scenarios and other tests not appropriate for vehicles.

### 3.2 dSpace HIL Simulator at Scania

The information in this chapter is taken from [3]. Scania PT is a HIL simulator developed by dSpace. It consists of 3 racks, see figure 3.1. Simulator rack 1 and 2 contains real-time system, signal conditioning, failure insertion units, loads and several different relays. The two simulator racks are then connected to the ECU-rack which contains the ECU:s and the Instrument Cluster (ICL).

The HIL simulator is hosted by a PC which has dSpace standard software and



**Figure 3.1.** *dSpace HIL simulator PT at Scania. From the left: Power supply, Simulator rack 1, ECU Rack, Simulator rack 2. The black cables connect the racks according to figure 3.2.*

ControlDesk, a user interface that controls the real-time hardware. More about ControlDesk in chapter 3.2.1. The PC and the two real-time systems are connected to each other via fibre optic cables.

The signal flow in the system is shown in figure 3.2. The three racks has the following contents:

- Simulator rack 1 contains model of Drivetrain (Retarder, Gearbox and Clutch) and related I/O for Gear Management System (GMS), All Wheel Drive (AWD), Clutch Control System (CLS) as well as Coordinator (COO).
- Simulator rack 2 contains model of Engine and related I/O for Engine Management System (EMS) as well as some other mandatory ECU: Instrument Cluster (ICL) and Exhaust Gas Aftertreatment System (EEC).
- ECU Rack holds the ECU:s, i.e. GMS, AWD, CLS, COO, EMS, ICL and EEC.

### 3.2.1 ControlDesk

Figure 3.3 shows the user interface ControlDesk. The numbered areas in the figure correspond to:

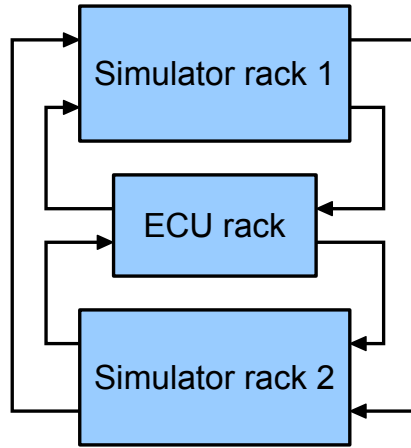


**Figure 3.2.** Schematic view of the signal flow between Simulator rack 1, Simulator rack 2 and the ECU rack in figure 3.1.

1. General Power Control – Controls the power supply, leftmost in figure 3.1.
2. Instrument Cluster – Shows engine speed, vehicle speed, chosen gear etc.
3. Gear selection – To change the gear in manual mode.
4. On/off key – Turns the ignition on and off.
5. Model information – Information about the chosen truck variant, as well as engine and gearbox configuration.
6. Pedal control - To change the accelerator pedal value.

The HIL simulator at Scania can either be controlled manually via ControlDesk user interface, or automatically via Python code. The validation part of this thesis has been done by a Python script that drives the HIL simulator and stores model variables in real-time. The automatic controlling is performed with the aid of TestAutomationFramework, a set of Python classes and methods that provides the basic functionality of a vehicle such as acceleration, braking, gear changes etc. There are also methods to emulate an engine placed in a testbench, these methods have also been used in this thesis.

### 3.2.2 Mean Value Engine Model

The model consists of the five blocks FuelSystem, PistonEngine, AirPath, ExhaustSystem and CoolingSystem, a schematic view is shown in figure 3.4. These are summarized in this section.

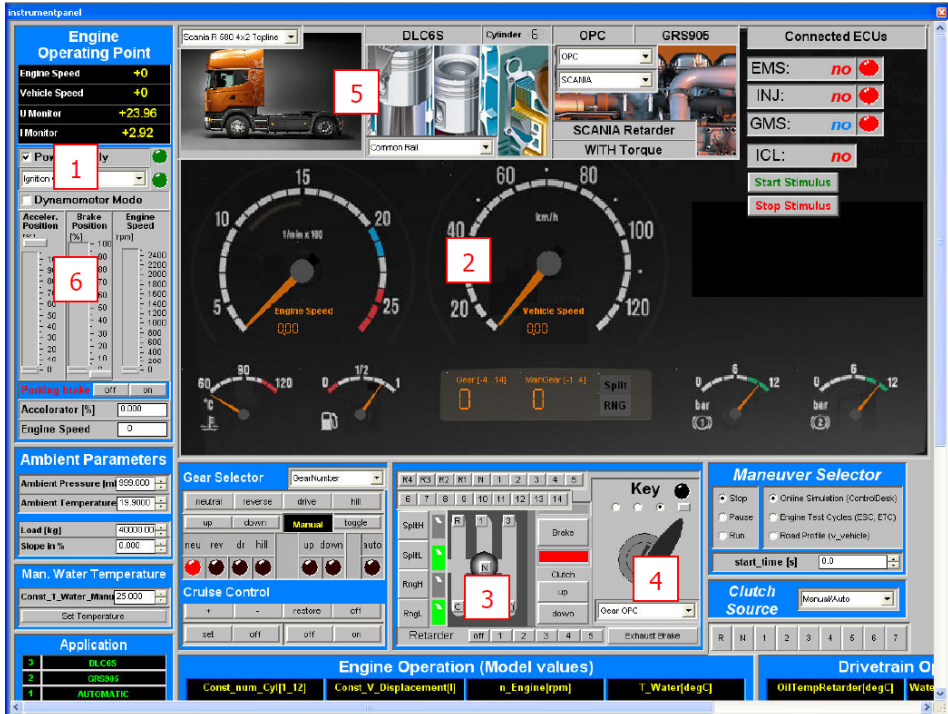


**Figure 3.3.** User interface ControlDesk. The HIL simulator at Scania can be controlled manually in this interface. It holds the basic functionality of a vehicle such as acceleration, brake and gear change. Information about the current vehicle as well as vehicle speed, engine speed and current gear are shown.

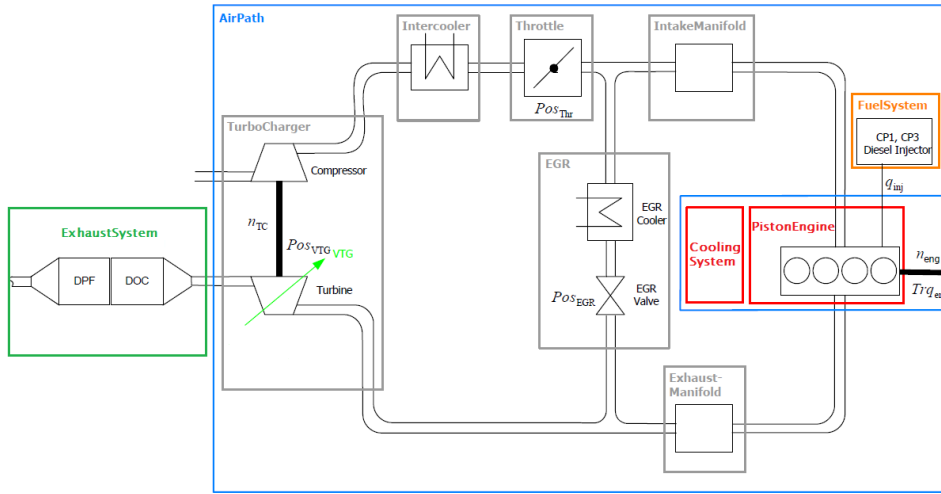


**Figure 3.4.** Overview of the engine model structure. This figure shows the five sub-blocks in the current engine: Fuelsystem, PistonEngine, AirPath, ExhaustSystem and CoolingSystem. The AirPath-block consists of the six blocks TurboCharger, Intercooler, Throttle, IntakeManifold, ExhaustManifold and EGR.

## FuelSystem

The block models the common-rail system which consists of several modules like the fuel tank, high pressure pump, fuel metering unit, pressure control valve and injector. A common-rail fuel system provides fuel for injection and the fuel is stored at high pressures in one chamber for all cylinders. This chamber is called the common rail. Common-rail systems enable fuel to be stored at high pressures independently of engine speed. The Simulink model FuelSystem is shown in figure A.1 on page 51.

## PistonEngine

The block PistonEngine describes the air flow through the inlet valve, the exhaust flow through the exhaust valve and the torque generated by the combustion process. In this case, the effective torque consists of the mean indicated torque and the friction torque. The effects of the injection angle and the air/fuel ratio are included as two efficiencies. The Simulink model PistonEngine is shown in figure A.2 on page 52.

## AirPath

This block simulates the compressor, intercooler, throttle and intake manifold dynamics on the intake side, and the turbine, EGR with cooler and exhaust manifold on the exhaust side. The turbocharger is modeled as a compressor and turbine connected via a turbocharger shaft. The intercooler cools the air flow from the

compressor according to the efficiency and temperature difference between the ambient and coolant temperature. The throttle is modeled as an orifice with a variable cross-section which limits the fresh air flow into the intake manifold. Mass balance is used to calculate the air mass in the intake manifold and the temperature of the manifold is calculated from energy balance. The pressure follows from the ideal gas law. Regarding the exhaust manifold, the same simulation approach is used. In contrast to the throttle, the mixing of fresh air with exhaust gas is calculated. The Simulink model AirPath is shown in figure A.3 on page 53.

### ExhaustSystem

The block ExhaustSystem describes the engine exhaust system. It contains models for a Diesel Oxidation Catalyst (DOC), Diesel Particulate Filter (DPF) and Selective Catalytic Reduction (SCR). DOC is used to reduce the amount of carbon monoxide ( $CO$ ) and unburned hydrocarbon ( $HC$ ), DPF for reducing particulates (soot) and the main task for the SCR is to reduce the nitrogen oxides ( $NO_x$ ). The Simulink model ExhaustSystem is shown in figure A.4 on page 54.

### CoolingSystem

The block CoolingSystem describes the engine cooling system. It calculates the cooling water temperature from the indicated mean torque and the friction torque. The system is modeled with a thermostat valve that regulates the cooling water temperature. The Simulink model CoolingSystem is shown in figure A.5 on page 55.

# Chapter 4

## Validation

### 4.1 Background

In the test cells at Scania CV, engine test benches are used to calibrate engines but also to ensure that the engines satisfy the specifications regarding torque, fuel consumption, emissions etc. In an engine test bench, the complete engine with aftertreatment system is driven in several different types of driving scenarios. Compared to engines in vehicles, a lot of extra sensors are mounted on the engine to be able to study the engine performance accurately. The validation in this thesis is done by comparing this kind of sensor data against data recorded in a HIL simulator. There are several different types of engine test procedures, but this thesis will focus on:

- Steady state – the engine is held at a constant load and speed for a desired amount of time.
- Transient – the engine speed and torque are varied throughout the test cycle.

#### 4.1.1 Dynamometer

In an engine test bench, the engine crankshaft is coupled to an electrical dynamometer as seen in figure 4.1. The dynamometer is an electric machine that can be used as a generator, when an external load is desired. But it can also drive the engine for measuring friction, pumping and acceleration losses. The dynamometer holds torque meter and tachometer that gives the possibility to measure the crankshaft torque and engine speed.

#### 4.1.2 PID controller

In this thesis, PID controllers are developed in Python in order to control the injected fuel quantity in the steady state validation and the crankshaft torque in the transient validation. In both cases, the control signal is the accelerator pedal value. In the second part of the steady state validation, the compressor flow is



**Figure 4.1.** A test bench in an engine test cell at Scania CV. The picture shows an engine (to the right) coupled to a dynamometer (to the left). The engine aftertreatment system is shown in the bottom left corner. It is connected to the outlet of the turbine as seen in the picture.

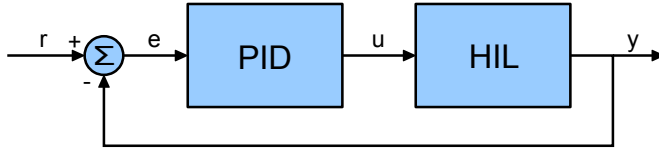


**Figure 4.2.** Schematic view of a PID controller. The control error ( $e$ ) is calculated as the difference between the system variable ( $y$ ) and the desired reference value ( $r$ ). The control signal ( $u$ ) to the system is then calculated by the PID controller.

controlled by adjusting the VGT-position. This is also done with a PID controller.

A Proportional-Integral-Derivative controller (PID-controller) is the most commonly used feedback controller. As seen in figure 4.2, the control error ( $e$ ) is calculated as the difference between measured system variable ( $y$ ) and desired reference value ( $r$ ) and given as input to the PID controller. The controller attempts to minimize this difference by adjusting the control signal ( $u$ ) to the system. The PID algorithm is defined as

$$u(t) = K_p e(t) + K_i \int_0^t e(t) dt + K_d \frac{d}{dt} e(t) \quad (4.1)$$

where  $K_p$ ,  $K_i$  and  $K_d$  are the proportional, integral and derivative gain parameters,  $e(t)$  is the control error ( $y(t) - r(t)$ ) and  $t$  the present time. The proportional term calculates an output that is proportional to the current error. This term can be adjusted by changing the proportional gain  $K_p$ . The integral term is the sum of



the instantaneous error over time, multiplied with the integral gain  $K_i$ . This term eliminates the steady state error that occurs with a pure proportional controller. The derivative term is calculated as the slope of the error over time, multiplied by the derivative gain  $K_d$ . This term slows the rate of the controller output, and is used to reduce the overshoot and to improve the stability of the PID-controller. The D-term is only used in the dynamic validation. The gain parameters for the PID-controller are tweaked manually to achieve the wanted controller behaviour. More detailed information about PID controllers can be found in [10].

## 4.2 Steady state validation

When performing steady state testing in an engine test cell, the engine speed is held constant with the aid of the dynamometer. Then, the accelerator pedal is used to achieve the wanted crankshaft torque. Increasing the accelerator pedal value leads to a higher fuel flow into the engine. Since the engine speed is held constant with the dynamometer, this will lead to an increasing engine torque. This scenario can be compared to driving uphill with a truck. In the opposite way, setting the accelerator pedal value to zero will shut off the fuel injection. In this case it will lead to a negative torque, since the engine will driven by the dynamometer.

### 4.2.1 Test data

The steady state engine data that is used in the validation part of this thesis is collected in an engine test cell at Scania CV. In figure 4.3, the crankshaft torque and engine speed from the stationary working points are shown. The engine is driven from 2300 rpm to 600 rpm and with different loads. In each stationary point, the engine is driven for 90 seconds, whereafter data is collected from the sensors mounted on it. To make a realistic comparison between engine test cell data and data from the HIL simulator, the engine model in the HIL simulator has to be driven in the same working points as the engine. In this thesis, this is achieved by controlling the engine speed with a simulated dynamometer, and simultaneously control the amount of injected fuel with a PI controller. A threaded Python script is developed for this task, where the engine speed and injected fuel are controlled in separate threads. After the specified stabilization time, the most important temperature, pressure, mass flow and torque values are measured.

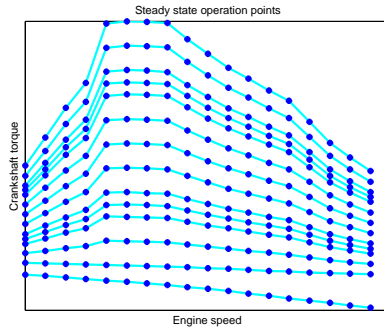


**Figure 4.3.** *Steady state operation points from engine test cell. The figure shows the 252 different combinations of engine speed and crankshaft torque that are used in the steady state validation. The topmost graph is the nominal torque limit, i.e. the maximum torque for different engine speeds.*

The engine speed and the injected fuel from the stationary working points are shown in figure 4.4. The first 18 values with large values on the injected fuel

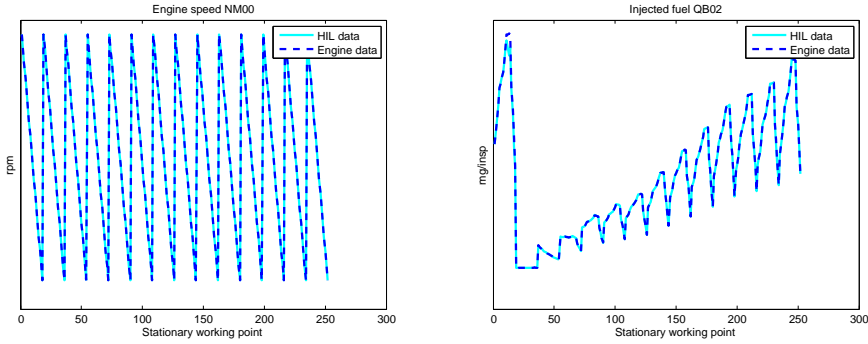


**Figure 4.4.** Simulated and measured engine speed and fuel quantity for the steady state operation points. These two variables are controlled in the Python script to emulate engine test cell data. The figures show that the automated controlling works well.

corresponds to the topmost graph in figure 4.3. As described in section 4.2, a large amount of injected fuel will lead to a high engine torque. The reason to the difference between the injected fuel in engine test cell and HIL simulator for the working points with the highest load is the nominal torque curve, which is the EMS torque limit for different engine speeds. When this limit is reached, the EMS will not increase the injected fuel quantity even though the accelerator pedal is pushed to the bottom.

The next 18 working points corresponds to the bottom graph in figure 4.3. In this region, the engine is driven entirely by the dynamometer and hence the fuel injection is shut off. The rest of the working points in figure 4.4 all corresponds to engine speeds in the interval 600-2300 rpm, with increasing values on the injected fuel.

### 4.2.2 Validation with controlled VGT and EGR positions

In figure 4.5, the VGT and EGR positions are shown when these are controlled entirely by the EMS. The figure shows that these positions have been controlled differently in the engine test cell and the HIL simulator. This is an indication to that the current engine model is not operating as the real engine, which makes the EMS to control the VGT and EGR differently. Figure 4.6 shows the difference between simulated and measured values. For the EGR valve, the deviation seems to be large at the high load points. The VGT seems to be controlled in the same way in some regions, but in others the difference is substantial. Altogether, the difference in VGT and EGR positions are too big to do a proper comparison between measurements from engine test cell and HIL simulator.

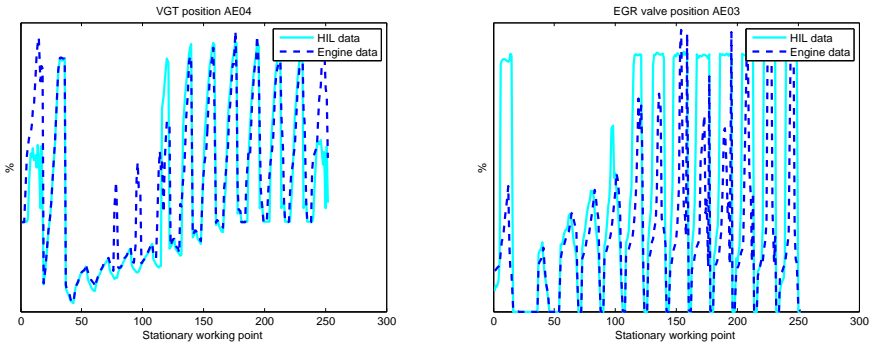


**Figure 4.5.** VGT and EGR positions, totally controlled by the EMS. The figure shows that the difference between simulated and measured VGT and EGR positions are large when these are controlled by the EMS.

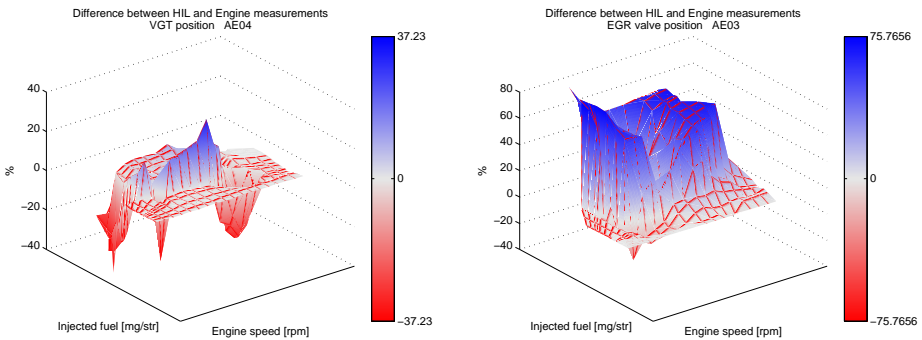


**Figure 4.6.** Difference between simulated and measured VGT and EGR positions. The figure shows in which operation points the largest deviation occurs.

The problem with different VGT and EGR positions in engine test cell and HIL simulator is solved by overriding the reference values for these positions in the EMS, which basically means that the requested positions are programmed in the control unit. The results can be seen in figure 4.7. Since these positions are controlled in real-time by the EMS, the requested values cannot be set directly in the model. This will cause diagnostic fault codes, due to that the EMS perceives that the EGR valve and VGT actuator are stuck.

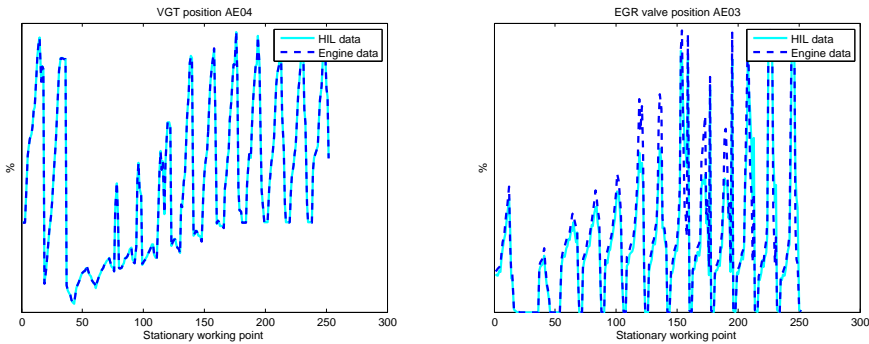


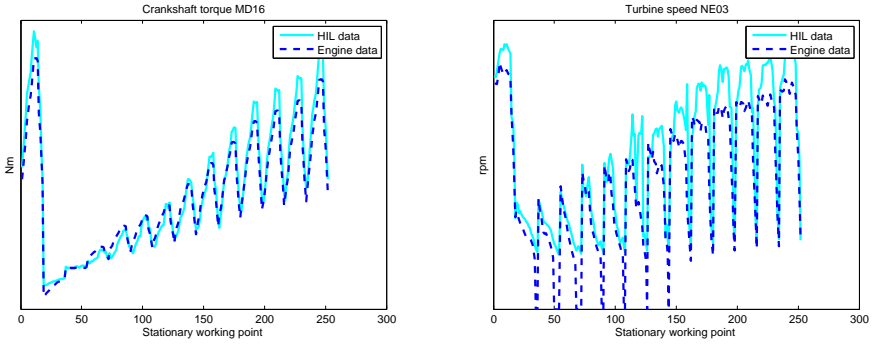
**Figure 4.7.** VGT and EGR positions, reference values in EMS overridden to emulate engine test bench data. Approximately the same positions are achieved for both VGT and EGR.

## Results

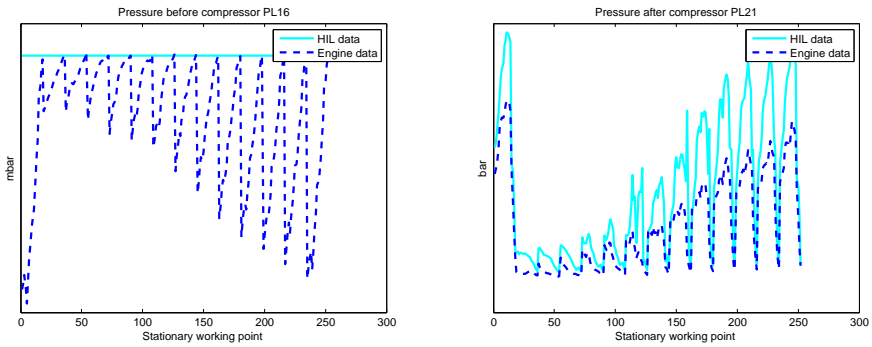
Figure 4.8 shows that the crankshaft torque is larger in the HIL simulator than in the real engine for the high load working points. This means that the modeled engine gives a larger torque output for the same amount of fuel at the same engine speed. This figure also shows that the simulated crankshaft torque is smaller for low loads. The pressure after the compressor is too high, especially for the high load working points, shown in figure 4.9. This also applies the pressure before the turbine in figure 4.10. In this figure, it can also be seen that the pressure after the turbine is too low in the HIL simulator.

Figure 4.11 shows the mass flow in to and out from the engine. First of all, it shall be noticed that there is a considerable difference between these flows in the engine test cell and the HIL simulator. The high compressor and turbine flow in the HIL simulator can be the source to the high pressures after the compressor and before the turbine. An increasing flow into the engine can lead to an increasing pressure.

The rest of the figures from the static validation with controlled VGT and EGR positions are shown in Appendix B on page 56. As for the compressor, the pressure after the intercooler and after the EGR cooler in figure B.1 and B.2 are higher for all working points in the HIL simulator. The compressor, EGR cooler and turbine temperatures are shown in figure B.3 – B.5. For the high load working



**Figure 4.8.** Crankshaft torque torque and turbine speed (values less than 20000 rpm are recorded as 0 in the engine test cell data). The torque is larger in the HIL simulator for almost every working point. A higher turbine speed is also recorded, especially in the high load working points.



**Figure 4.9.** Pressure before and after compressor. The pressure after the compressor is nearly two times larger in the HIL simulator for the high load working points.

points, the temperature after the compressor is too high in the HIL simulator. The temperature after the EGR cooler shows a large deviation from engine test cell data, but the temperature before and after the turbine seems to be modeled correctly. Regarding the flow through the EGR valve in figure B.6, in the high load working points this value is nearly two times larger in the HIL simulator. This is probably due to the high pressures in the exhaust manifold. Furthermore, this flow turns negative in some working points in the HIL simulator. This means that the air is flowing from the intake manifold, through the EGR valve into the exhaust manifold. This is a consequence of the control of EGR positions, the EGR valve should normally be closed when the pressure is higher in the inlet than in the outlet of the engine.

From these figures, it is obvious that the relationship between pressure and flow

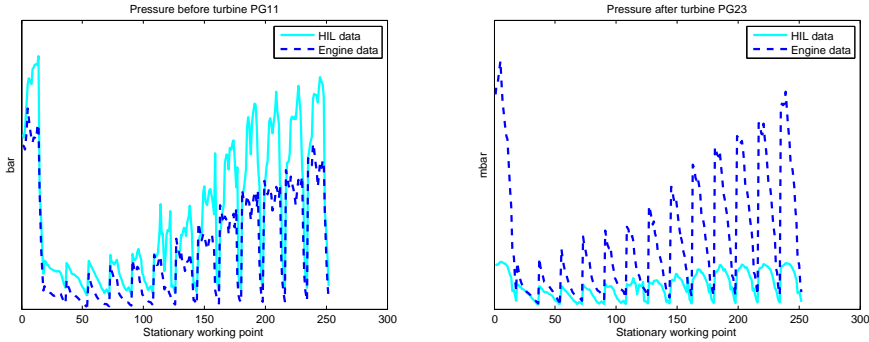


**Figure 4.10.** *Pressure before and after turbine. For the HIL simulator, the pressure before the turbine is remarkable high.*

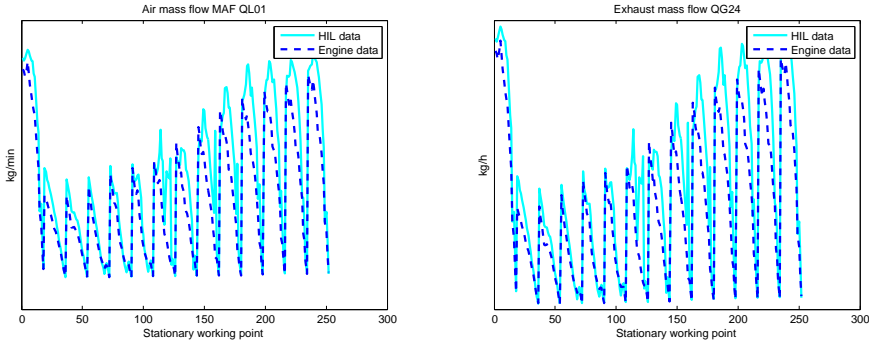


**Figure 4.11.** *Compressor and turbine flow. These flows are approximately equal since the engine is driven stationary. For both compressor and turbine, the flow is larger in the HIL simulator at almost every working point.*

in the HIL simulator is modeled poorly. However, it is not possible to isolate the faulty component by analysing these plots. This is due to that a large mass flow into the engine will cause a large mass flow out from the engine since the engine is driven stationary. An increasing flow through the turbine will lead to an increasing turbine speed, and consequently the compressor will compress more air into the engine. The next step of the steady state validation is therefore to control the VGT position in order to achieve the same inlet mass flow in engine and HIL simulator. With this approach, the component that causes these errors can more easily be isolated.

### 4.2.3 Validation by controlling the intake flow with the VGT position

As seen in figure 4.11 on page 23, there are large compressor and turbine flows in the HIL simulator compared to the engine test cell for almost every stationary working point. The fact that the VGT and EGR positions are the same indicates that there is something wrong with the current engine model. However, it is not possible to isolate the faulty component since the turbine and compressor are connected mechanically by the turbine shaft. To isolate the inlet from the outlet, the VGT position is used to control the air flow into the engine. This is done with a PI-controller that is tweaked manually to achieve the wanted control performance. The EGR position is controlled in the same way as in section 4.2.2. The resulting VGT and EGR positions can be seen in figure 4.12.

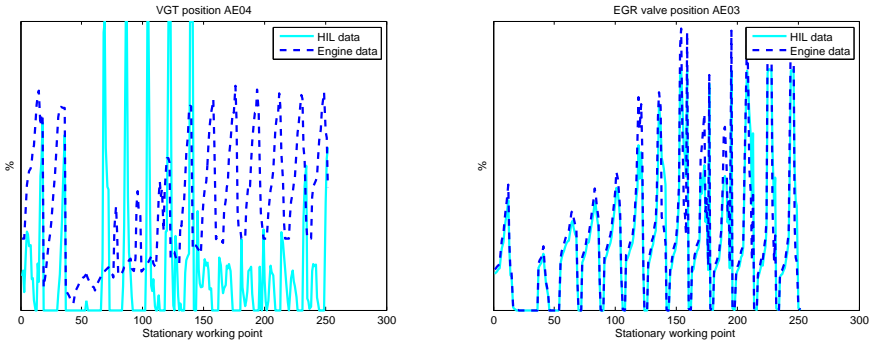


**Figure 4.12.** VGT and EGR positions, when the VGT position is varied to achieve the same compressor flow in the HIL simulator and the engine test cell. The EGR is controlled to emulate data from the engine test cell. As seen in the left figure, it takes a completely different VGT position in the HIL simulator to achieve the same compressor flow.

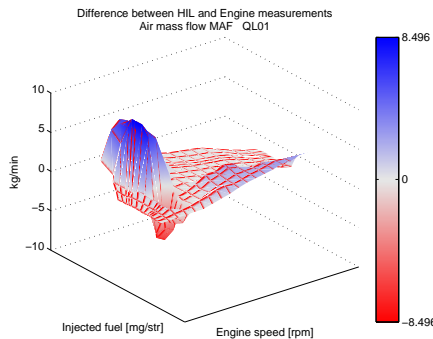


**Figure 4.13.** Difference between compressor flow in engine test cell and HIL simulator when the VGT position is used to control the flow. The figure shows that the same compressor flow can only be achieved in the working points with high load and high engine speed.



## Results

The inlet and outlet flow can be seen in figure 4.14. Noteworthy is that the same compressor flow can only be achieved in the working points with high load and high engine speed, see figure 4.13. The compressor flow, and thereby the turbine flow, is too high in the HIL simulator for the stationary working points with low load and in the high load points with low engine speed. In these cases the VGT position in figure 4.12 is zero, which means that the effective area in the turbine has reached its maximum value. This corresponds to that a relatively small amount of the energy in the exhaust gases are used to drive the compressor. Regarding the regions where the compressor flow in figure 4.14 is too small, this behaviour is seen in the working points with low load and low engine speed. In these cases the VGT position in figure 4.12 has reached its maximum value and the effective area is thereby as small as possible. This means that a large amount of the energy in the exhaust gases are used to compress the intake air flow. Despite this, the mass flow through the compressor is too small. In these points, the correct amount of fuel is not reached, see figure 4.15.

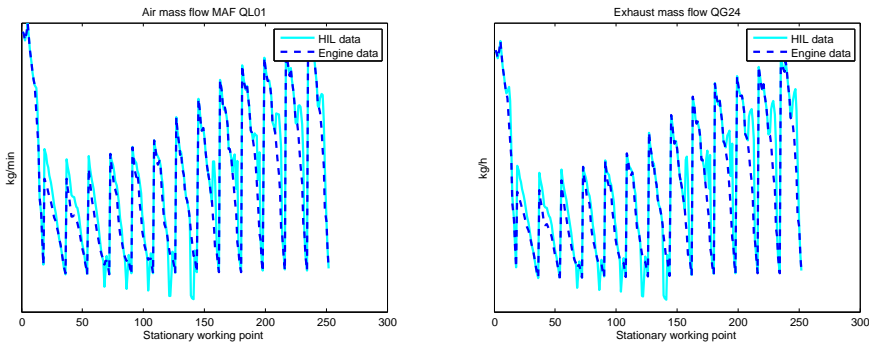


**Figure 4.14.** Compressor and turbine flow when the VGT position is used to control the flow. The figure shows that the same compressor flow cannot be achieved in every working point.

The pressure after the compressor and before the turbine in figure 4.16 and 4.17 seems to be correct except from the working points where the inlet flow is too high. In the stationary points where VGT position is set to zero and the compressor flow is too high according to the reasoning above, the pressures in the inlet and outlet of the engine will increase. This is due to the increased air flow into the engine.

In Appendix C on page 59, the rest of the figures from the validation in this section are shown. Figure C.1 shows approximately the same turbine speed in the working points with the same mass flow in HIL simulator and engine test cell. The intercooler and EGR cooler pressures in figure C.2 and C.3 shows a good fit in the working points with correct mass flow. This also applies the temperatures in figure C.4 – C.6, except from the temperature after the EGR cooler. An important

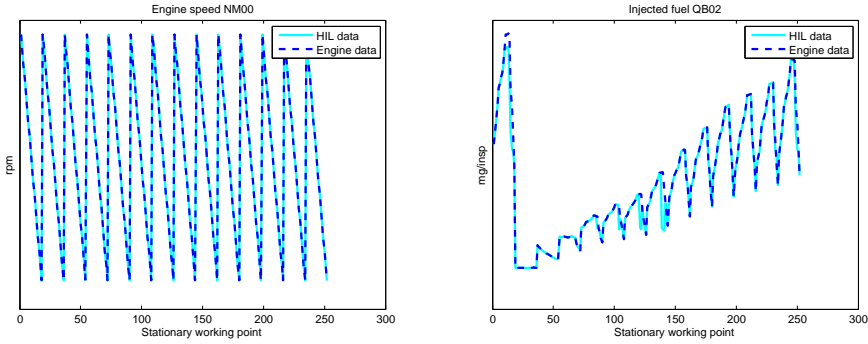


**Figure 4.15.** Engine speed and injected fuel. In the middle of the right figure, there is a large deviation in injected fuel for some working points. This is a consequence of a too small air flow into the engine, see figure 4.14.

notice from the temperature after the compressor in figure C.4 is that a too high mass flow will lead to a too high temperature.

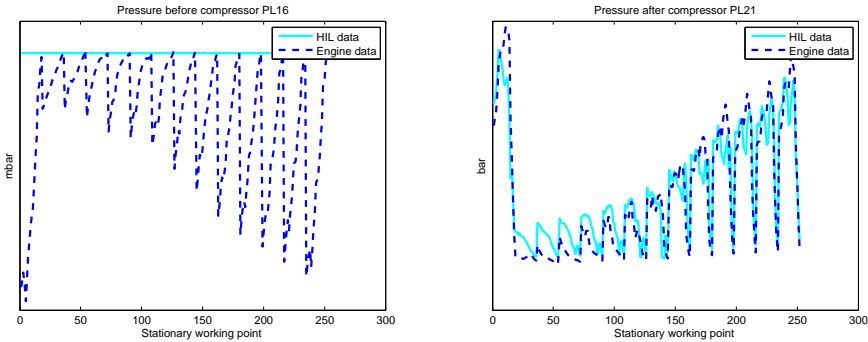


**Figure 4.16.** Pressure before and after compressor. The pressure after the compressor shows a good fit in the working points with the correct flow.

The rest of this validation section will focus on the stationary points where the same compressor flow in HIL simulator and engine is achieved. For example stationary point 181-189, which corresponds to engine speeds in the interval 2300-1600 rpm and loads around 70 per cent of nominal torque.

The compressor and turbine mass flows are the same for HIL and engine measurements, shown in figure 4.19 and 4.20. In figure 4.18, the VGT position and turbine speed is shown for working point 180-190. The difference in turbine speed is small for high engine speeds, and increases with decreasing values on the engine speed. The turbine speed is although lower in the HIL simulator for each value

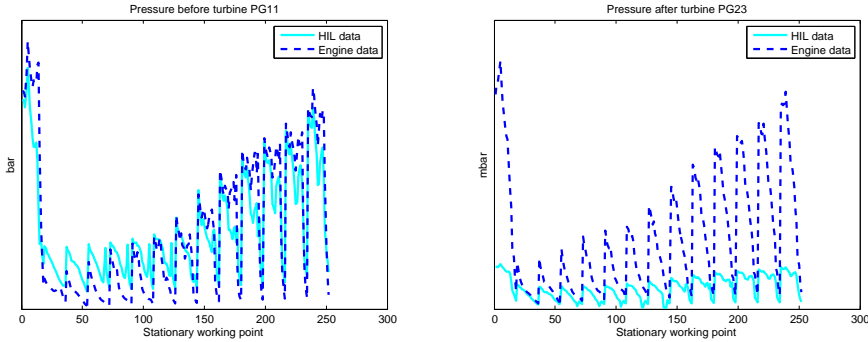


**Figure 4.17.** Pressure before and after turbine. The pressure before the turbine shows a good fit in the regions where the same compressor flow in HIL simulator and engine test cell is achieved.

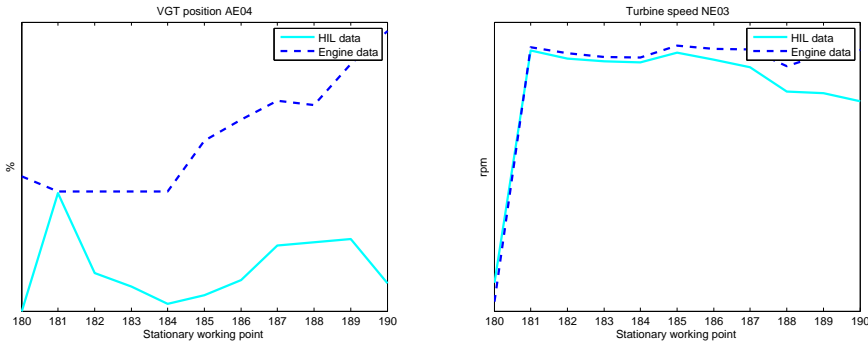


**Figure 4.18.** VGT position and turbine speed for the stationary working points 180-190. The VGT position is smaller in the HIL simulator for every working point except 181. The turbine speed is approximately equal for the working points 180-185.

in the specified interval. This means that the same mass flow requires a lower turbine speed in the HIL simulator. The pressure after the compressor, shown in figure 4.19, is higher in the HIL simulator when the difference in turbine speed is small. When this difference increases, the pressure in the HIL simulator becomes lower than the pressure in the real engine. An important conclusion from this reasoning is that the same compressor flow and approximately the same turbine speed leads to a too high pressure after the compressor in the HIL simulator. The compressor model, that calculates the pressure out from the compressor, causes the deviation. This model needs to be modified so that the relationship between compressor flow, turbine speed and pressure after the compressor becomes correct.

The pressure before the turbine and the turbine mass flow is shown in figure 4.20. The difference in pressure increases with decreasing engine speeds. For the

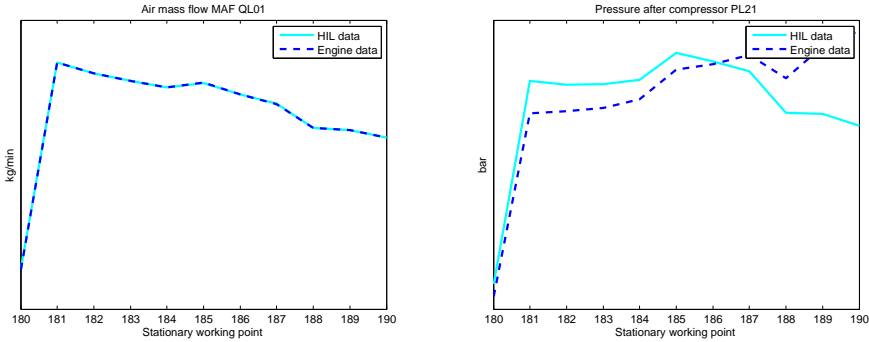


**Figure 4.19.** Compressor mass flow and pressure after compressor for the stationary working points 180-190. The compressor mass flow is the same in HIL simulator and engine test cell for every working point in the specified interval. The pressure after the compressor is higher in the HIL simulator for working point 180-185, where the turbine speed is approximately equal (figure 4.18).

points 181-185, the same turbine flow and approximately the same turbine speed are measured. The VGT positions in these points are considerably smaller in the HIL simulator, which corresponds to a large relative turbine area and thereby that a small amount of the energy in the exhaust gases are used to drive the compressor. Consequently, approximately the same turbine speed can be achieved with the same turbine mass flow and a larger turbine area. This conclusion shows that a new turbine model with the correct VGT behaviour needs to be implemented.

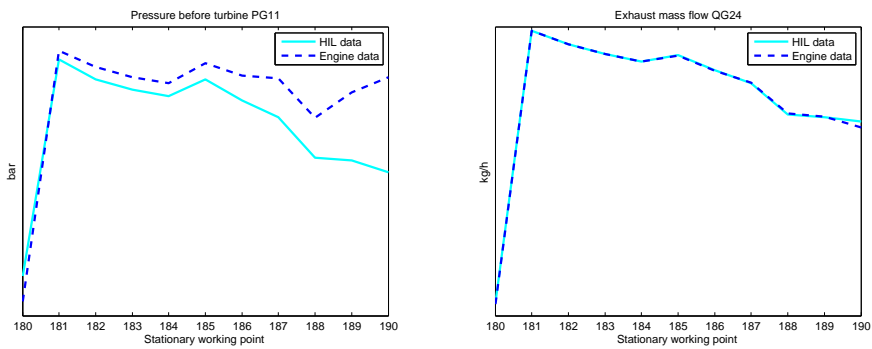


**Figure 4.20.** Pressure before turbine and turbine mass flow for the stationary working points 180-190. The figure shows that the same turbine mass flow requires a lower pressure before the turbine for every working point in the specified interval.

#### 4.2.4 Validation of compressor and turbine model

The existing compressor and turbine model are simulated outside the HIL environment, with inputs from the stationary measurements in engine test cell. The inputs to the models can be seen in table 4.1. Low turbine speeds are hard to

Compressor input	Turbine input
Pressure before compressor, $p_{bc}$	Pressure before turbine, $p_{em}$
Temperature before compressor, $T_{bc}$	Pressure after turbine, $p_t$
Compressor mass flow, $W_c$	Temperature before turbine, $T_{em}$
Turbine speed, $\omega$	VGT control signal, $u_{vgt}$
	Turbine speed, $\omega$

**Table 4.1.** Inputs to the existing turbo model.

measure accurately. In the data from the engine test cell, all measured turbine speeds below 20 000 rpm has been documented as 0 rpm since the uncertainty is too high. These data points have been removed in this validation. The outputs, except from the compressor and turbine power, can be seen in figure 4.21 and 4.22. For the compressor, the pressure out is too high for the HIL simulator in

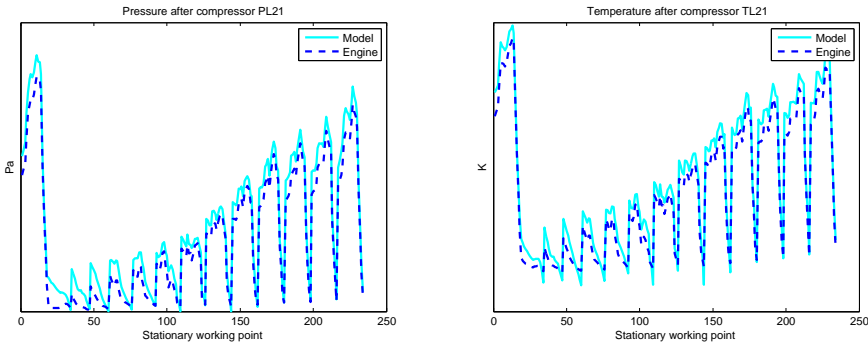


**Figure 4.21.** Pressure and temperature after compressor when the current compressor model is simulated with data from engine test cell. Both of these variables are larger in the HIL simulator for almost every working point.

every working point, especially in the low load points. This is definitely one main reason to the high pressures in the rest of the modeled engine. The compressor out temperature is also higher in the HIL simulator, but this is acceptable since the overall temperatures in the modeled engine shows a good fit to measured data. This also applies to the temperature after the turbine, but the turbine mass flow shows a large deviation from engine data. Especially for low loads and high loads with low engine speeds. In this case, it takes a smaller turbine mass flow to achieve the same turbine speed at the same VGT control signal. This conclusion coincides

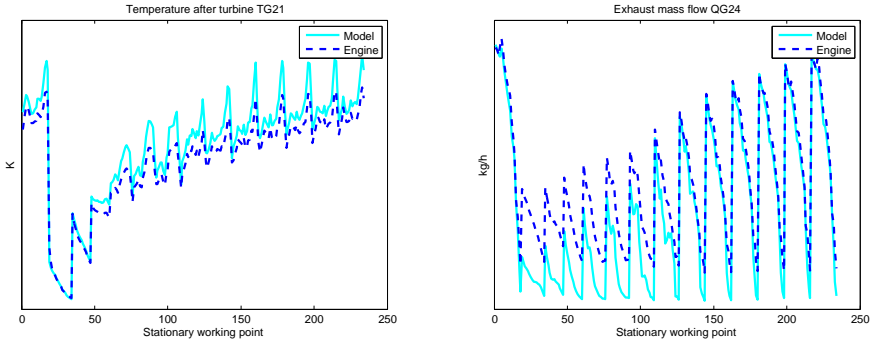


**Figure 4.22.** Temperature after the turbine and turbine mass flow when the current turbine model is simulated with data from engine test cell. As for the compressor, the temperature after the turbine is larger in the HIL simulator. The turbine mass flow shows a large deviation from engine test cell data, especially for low loads. This is seen in the right figure.

with the results from section 4.2.3, where the same mass flow was achieved with the same area but a smaller turbine speed in the HIL simulator.

### 4.3 Transient validation

The World Harmonized Transient Cycle (WHTC) is used for the transient validation in this thesis. This cycle is a transient test of 1800 seconds, with several motoring segments. The engine speed and the crankshaft torque are varied throughout the test cycle, see figure 4.23. As in the steady state validation, a simulated dynamometer is used to control the engine speed. The crankshaft torque is controlled with a PID controller, where the accelerator pedal is the control signal. These two variables are controlled in separate threads in a Python script. However, the crankshaft torque signal needs to be filtered, to smooth out high frequent noise. Therefore, a lowpass filter is implemented:

$$y(t_k) = (1 - a)y(t_{k-1}) + au(t_k) \quad (4.2)$$

where the filter parameter  $a$  is a function of the time step  $h$  and the filter constant  $T_f$  according to

$$a = \frac{h}{T_f + h} \quad (4.3)$$

The present filter output  $y(t_k)$  is consequently a function of the present filter input  $u(t_k)$  and the filter output at the previous discrete time  $y(t_{k-1})$ . When the parameter  $a$  is close to 1, the input and output to the filter are approximately the same and the filter response is thereby fast. When the value on  $a$  decreases, the filter output will be more dependent on previous outputs and the filter response is thereby slower. The result from the low pass filtering of the crankshaft torque signal can be seen in figure 4.24.

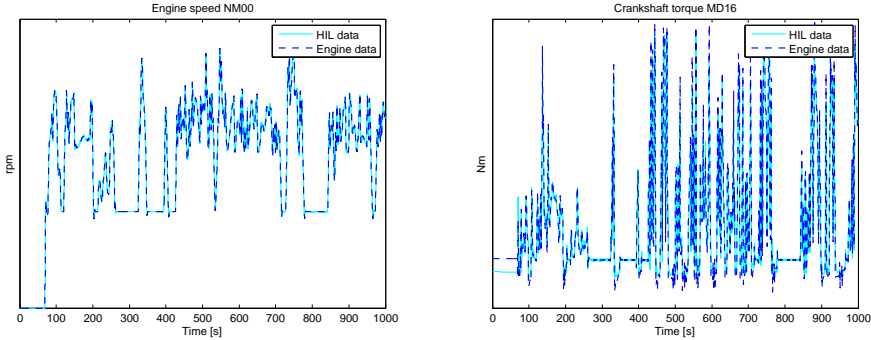


**Figure 4.23.** Engine speed and crankshaft torque for the first 1000 seconds of the WHTC cycle. These two variables are controlled in separate threads in a Python script. The figures show that the automated controlling works well.

The engine speed and crankshaft torque for the time interval 400-600 seconds can be seen in figure 4.25. These figures show that the dynamic validation method works fine. The VGT and EGR positions are controlled to emulate engine test bench data, shown in figure 4.26.



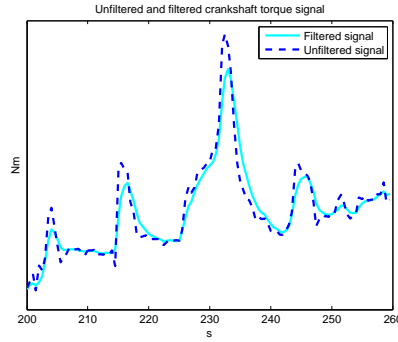


**Figure 4.24.** Filtered and unfiltered crankshaft torque signal. The lowpass filtering is necessary since the crankshaft torque signal is used as measurement signal to the PID controller.

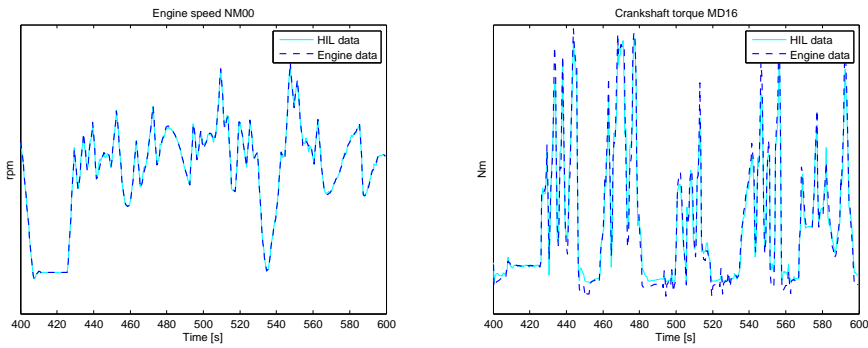


**Figure 4.25.** Engine speed and crankshaft torque. These variables are controlled in separate threads in the Python script, the figures show that the controlling works well.

## Results

As in the steady state validation, the compressor and turbine flow in figure 4.27 are larger in the HIL simulator than in the engine. The pressure in the intake manifold in figure D.1 on page 63 is higher, but the pressure after the turbine in figure D.2 is lower. Regarding the temperature after the compressor in figure D.3, it can be seen that this value changes too fast in the HIL simulator. In the real engine, the temperature changes slowly even though the turbine speed in figure D.4 shows a fast response. The time constant of the temperature sensor mounted in the engine test cell can be the source to this deviation.

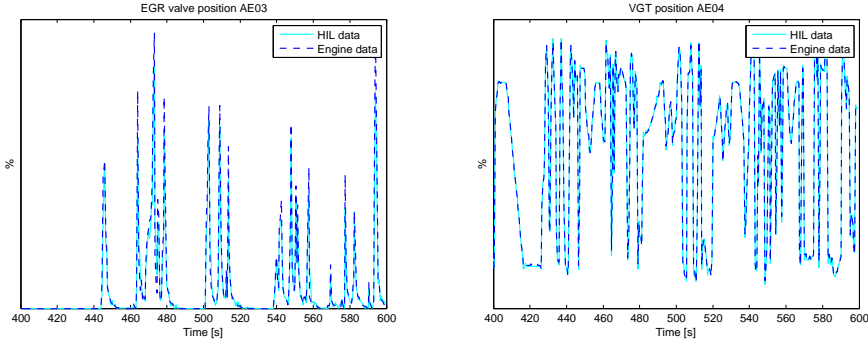


**Figure 4.26.** VGT and EGR positions. In the HIL simulator, these positions are controlled to emulate engine test cell data. The figure shows that this works well.

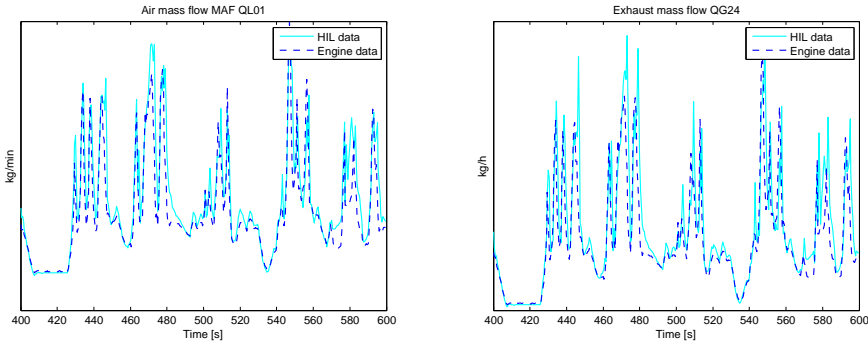


**Figure 4.27.** Inlet and exhaust flow. The flows are slightly larger in the HIL simulator. This coincides with the results from the steady state validation.

# Chapter 5

## Turbocharging

A turbocharger normally consists of a centrifugal compressor and a radial turbine. The turbine and the compressor are mechanically coupled to each other via a shaft. The turbine utilizes the energy in the exhaust gases to drive the compressor which is used to compress the intake air flow. The performance of a turbocharger is usually represented by a map that connects the shaft speed and pressure ratio to the mass flow and efficiency, see figure 5.1. These maps are often provided by the manufacturer, to describe the performance of the turbine and compressor. A more detailed explanation of the variables used in this map is given in section 5.1.1 and 5.2.1. The equations in this chapter are collected from [7].

The maximum flow through the compressor is limited by the choke line, shown in the lower right corner of the compressor map. To the left of the surge line, the compressor flow is unstable. When the pressure ratio over the compressor becomes too high, the flow reverses in the compressor and the pressure generated by the compressor is thereby limited.

### 5.1 Turbine performance

A turbine drives the turbo shaft by expanding gases from a higher temperature and pressure to a lower temperature and pressure. The turbine power is defined as

$$P_t = W_t c_{pe} (T_{em} - T_t) \quad (5.1)$$

where  $W_t$  is the turbine mass flow flow,  $c_{pe}$  the specific heat capacity for exhaust gas,  $T_{em}$  the temperature in the exhaust manifold and  $T_t$  the temperature after the turbine. The power from the isentropic process is defined as

$$P_{t,s} = W_t c_{pe} (T_{em} - T_{t,s})$$

where  $T_{t,s}$  is the temperature after the turbine for the isentropic process. The quotient between the temperature after and before the turbine can be represented

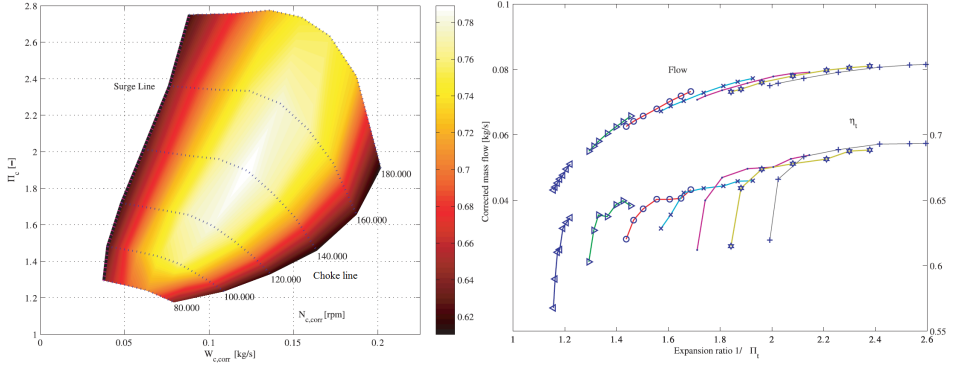


**Figure 5.1.** Left: Compressor map. The speed lines  $N_{c,corr}$  show how the pressure ratio  $\Pi_c$  and corrected mass flow  $W_{c,corr}$  are connected to the efficiency  $\eta_c$  for constant speeds. The area in the middle of the map with the brightest color shows where the compressor is most effective. Right: Turbine map. Shows how the expansion ratio  $\frac{1}{\Pi_t}$  is connected to the corrected turbine mass flow  $W_{t,corr}$  (left y-axis) and efficiency  $\eta_t$  (right y-axis) for different constant speeds. Both figures are taken from [6].

as a function of the pressure after and before the turbine according to

$$\frac{T_{t,s}}{T_{em}} = \left( \frac{p_t}{p_{em}} \right)^{1-1/\gamma_e} = \Pi_t^{1-1/\gamma_e}$$

where  $\gamma_e$  is the isentropic expansion factor for exhaust gas. This leads to the following expression for the power for the isentropic process.

$$P_{t,s} = W_t c_{pe} T_{em} \left( 1 - \Pi_t^{1-1/\gamma_e} \right) \quad (5.2)$$

The turbine efficiency is defined as the actual power delivered, divided by the power delivered from an isentropic process, which gives the following expression for the turbine efficiency

$$\eta_t = \frac{P_t}{P_{t,s}} = \frac{T_{em} - T_t}{T_{em} \left( 1 - \Pi_t^{1-1/\gamma_e} \right)} \quad (5.3)$$

However, in equation 5.3, it is assumed that there are no heat losses in the turbine. This leads to errors if this equation is used to calculate the turbine efficiency. In [16], another efficiency is used that is approximately equal to  $\eta_t$ . At steady state, the turbine and compressor power are approximately equal, which gives the following efficiency

$$\eta_{tm} = \eta_t \eta_m = \frac{P_c}{P_{t,s}} = \frac{W_c c_{pa} (T_c - T_{bc})}{W_t c_{pe} T_{em} \left( 1 - \Pi_t^{1-1/\gamma_e} \right)} \quad (5.4)$$

This efficiency is often used as the turbine efficiency. However, an important notice is that this term also includes the mechanical efficiency  $\eta_m$ .

### 5.1.1 Turbine map

The turbine map consists of four performance variables: expansion ratio, corrected mass flow, corrected turbine speed and turbine efficiency. The corrected turbine mass flow is given by

$$W_{t,corr} = W_t \sqrt{\frac{T_{em}}{T_{t,ref}}} \frac{p_{em}}{p_{t,ref}} \quad (5.5)$$

where  $T_{t,ref}$  and  $p_{t,ref}$  are nominal temperature and pressure that are used to normalize the performance. The corrected shaft speed is defined as

$$N_{t,corr} = N_t \sqrt{\frac{T_{t,ref}}{T_{em}}} \quad (5.6)$$

The turbine pressure ratio is given by the pressure after the turbine divided by the pressure before the turbine according to

$$\Pi_t = \frac{p_t}{p_{em}} \quad (5.7)$$

but in the turbine map, the expansion ratio (inverted pressure ratio) is often used

$$\frac{1}{\Pi_t} = \frac{p_{em}}{p_t} \quad (5.8)$$

## 5.2 Compressor performance

Analogically to equation 5.1-5.3, the compressor power, isentropic power and efficiency are given by equations 5.9-5.11. The power is thereby defined as

$$P_c = W_c c_{pa} (T_c - T_{bc}) \quad (5.9)$$

where  $c_{pa}$  is the specific heat capacity for air. The power from the isentropic process is given by

$$P_{c,s} = W_c c_{pa} (T_{c,s} - T_{bc})$$

where the temperature quotient can be represented by

$$\frac{T_{c,s}}{T_{bc}} = \left( \frac{p_{c,s}}{p_{bc}} \right)^{1-1/\gamma_a} = \Pi_c^{1-1/\gamma_a}$$

where  $\gamma_a$  is the isentropic expansion factor for air. This gives the ideal compressor power

$$P_{c,s} = W_c c_{pa} T_{bc} \left( \Pi_c^{1-1/\gamma_a} - 1 \right) \quad (5.10)$$

The compressor efficiency is thereby defined as

$$\eta_c = \frac{P_{c,s}}{P_c} = \frac{T_{bc} \left( \Pi_c^{1-1/\gamma_a} - 1 \right)}{T_c - T_{bc}} \quad (5.11)$$

### 5.2.1 Compressor map

The compressor map also consists of four performance variables: corrected mass flow, corrected shaft speed, pressure ratio and compressor efficiency. The corrected compressor mass flow is given by

$$W_{c,corr} = W_c \frac{\sqrt{\frac{T_{bc}}{T_{c,ref}}}}{\frac{p_{bc}}{p_{c,ref}}} \quad (5.12)$$

where  $T_{c,ref}$  and  $p_{c,ref}$  are nominal temperature and pressure. The corrected shaft speed is described as

$$N_{c,corr} = N_t \frac{1}{\sqrt{\frac{T_{bc}}{T_{c,ref}}}} \quad (5.13)$$

and the compressor pressure ratio by

$$\Pi_c = \frac{p_{ac}}{p_{bc}} \quad (5.14)$$

## 5.3 Turbo Dynamics

The losses in the shaft that connects the turbine and the compressor are defined as the mechanical efficiency,  $\eta_m$ . At steady state, the relationship between the turbine and compressor power can be described by the equation

$$\eta_m P_t = P_c \quad (5.15)$$

The turbo speed,  $\omega_t$ , is modeled using Newton's second law:

$$\frac{d\omega}{dt} = \frac{1}{J_t} \left( \frac{P_t}{\omega} \eta_m - \frac{P_c}{\omega} \right) \quad (5.16)$$

or, according to [6]

$$\frac{d\omega}{dt} = \frac{1}{J_t} \left( \frac{P_t}{\omega} - \frac{P_c}{\omega} - M_{fric}(\omega) \right) \quad (5.17)$$

where the mechanical efficiency  $\eta_m$  has been replaced by the friction torque,  $M_{fric}(\omega)$ . This is a quadratic function of rotational speed, and  $\omega$  is the angular velocity given by the relationship  $\omega = 2\pi N$ .

# Chapter 6

## Modeling

In this chapter, a variable geometry turbine is modeled. The model consists of the two submodels mass flow and turbine efficiency.

### 6.1 Existing turbine model

The inputs and outputs in the existing turbine model are specified in table 6.1 and 6.2. Equation 5.1 is used to calculate the turbine power:

$$P_t = W_t c_{pe} (T_{em} - T_t) \quad (6.1)$$

where the temperature after the turbine is derived from equation 5.3 on page 36 which gives

$$T_t = T_{em} \left( 1 - \eta_t \left( \Pi_t^{1-1/\gamma_e} - 1 \right) \right) \quad (6.2)$$

The turbine mass flow is derived from equation 5.5

$$W_t = \frac{\left( \frac{p_{em}}{p_{t,ref}} \right) W_{t,corr}}{\sqrt{\frac{T_{em}}{T_{t,ref}}}} \quad (6.3)$$

The turbine efficiency  $\eta_t$  and the corrected mass flow  $W_{t,corr}$  are derived from a turbine map similar to figure 5.1 on page 36. In this case six different turbine maps are used, each map is valid for a specified interval on the VGT actuator position  $u_{vgt}$ . The input values to the map interpolation are the corrected shaft speed in equation 5.6 and the expansion ratio in equation 5.8.

### 6.2 Turbine model

The turbine power and temperature out from the turbine are modeled as in section 6.1. However, in this section semi-physical mathematical models for the turbine efficiency and the turbine mass flow are presented.

Input	Description	Unit
$\omega_t$	Turbine speed	[rpm]
$p_{em}$	Pressure exhaust manifold	[Pa]
$p_t$	Pressure after turbine	[Pa]
$T_{em}$	Temperature exhaust manifold	[°C]
$u_{vgt}$	VGT control signal [0-1]	[-]

**Table 6.1.** Inputs to the existing turbine model.

Output	Description	Unit
$P_t$	Turbine power	[W]
$T_t$	Temperature after turbine	[K]
$W_t$	Turbine mass flow	[kg/s]

**Table 6.2.** Outputs from the existing turbine model.

### 6.2.1 Turbine mass flow

The turbine mass flow is modeled according to [16]

$$W_t = \frac{A_{vgtmax} p_{em} f_{\Pi_t}(\Pi_t) f_{vgt}(u_{vgt})}{\sqrt{T_{em} R_e}} \quad (6.4)$$

where the  $A_{vgtmax}$  is the maximum area in the turbine that the gas flows through.  $R_e$  is the ideal gas constant for exhaust gas. When the pressure ratio  $\Pi_t$  decreases, the mass flow increases until the gas reaches the sonic condition and the flow is choked. The behaviour can be described by a non-physical choking function

$$f_{\Pi_t}(\Pi_t) = \sqrt{1 - \Pi_t^{K_t}} \quad (6.5)$$

When the VGT control signal  $u_{vgt}$  increases, the effective area in the turbine increases and consequently the flow through the turbine increases. The geometry in the turbine causes a large change in the effective area when the VGT control signal is small. This can be described by a part of an ellipse

$$\left[ \frac{f_{vgt}(u_{vgt}) - c_{f1}}{c_{f1}} \right]^2 + \left[ \frac{u_{vgt} - c_{vgt2}}{c_{vgt1}} \right]^2 = 1$$

which leads to the following expression for the effective area ratio function

$$f_{vgt}(u_{vgt}) = c_{f2} + c_{f1} \sqrt{\max(0, 1 - \left( \frac{u_{vgt} - c_{vgt2}}{c_{vgt1}} \right)^2)} \quad (6.6)$$

### Tuning parameters

The parameters in the mass flow model that are tuned:



- $K_t$  in equation 6.5
- $c_{f1}$ ,  $c_{f2}$ ,  $c_{vgt1}$  and  $c_{vgt2}$  in equation 6.6

These parameters are tuned according to section 6.2.3 and validated in section 6.2.4.

### 6.2.2 Turbine efficiency

The turbine efficiency is modeled according to [15]. Measurements show that the turbine efficiency in equation 5.4 depends on the Blade Speed Ratio (BSR), VGT position and the turbine speed. The turbine efficiency is therefore modeled as a product of three efficiencies

$$\eta_{tm} = \eta_{tm,BSR}(BSR) \cdot \eta_{tm,\omega_t}(\omega_t) \cdot \eta_{tm,u_{vgt}}(u_{vgt}) \quad (6.7)$$

The first efficiency  $\eta_{tm,BSR}(BSR)$  is modeled as a parabolic function with a square on the input variable  $BSR$

$$\eta_{tm,BSR}(BSR) = 1 - b_{BSR}(BSR^2 - BSR_{opt}^2)^2 \quad (6.8)$$

where the blade speed ratio  $BSR$  is the quotient of the turbine blade tip speed and the speed which a gas reaches when expanded isentropically at a given pressure ratio  $\Pi_t$

$$BSR = \frac{R_t \omega_t}{\sqrt{2c_{pe}T_{em} \left(1 - \Pi_t^{1-1/\gamma_e}\right)}}$$

where  $R_t$  is the turbine blade radius. The second efficiency  $\eta_{tm,\omega_t}(\omega_t)$  describes the mechanical losses in the turbine. Measurements show that these losses are large at low turbine speeds, therefore this efficiency is modeled as two linear functions in two different regions

$$\eta_{tm,\omega_t}(\omega_t) = \begin{cases} 1 - b_{\omega t1}\omega_t & \text{if } \omega_t \leq \omega_{t,lim} \\ 1 - b_{\omega t1}\omega_{t,lim} - b_{\omega t2}(\omega_t - \omega_{t,lim}) & \text{if } \omega_t > \omega_{t,lim} \end{cases} \quad (6.9)$$

The third efficiency is modeled as a third order polynomial

$$\eta_{tm,u_{vgt}}(u_{vgt}) = b_{vgt1}u_{vgt}^3 + b_{vgt2}u_{vgt}^2 + b_{vgt3}u_{vgt} + b_{vgt4} \quad (6.10)$$

### Tuning parameters

The parameters in the efficiency model that are tuned:

- $b_{BSR}$  and  $BSR_{opt}$  in equation 6.8
- $b_{\omega t1}$ ,  $b_{\omega t2}$  and  $\omega_{t,lim}$  in equation 6.9
- $b_{vgt1}$ ,  $b_{vgt2}$ ,  $b_{vgt3}$  and  $b_{vgt4}$  in equation 6.10

These parameters are tuned according to section 6.2.3 and validated in section 6.2.4.

### 6.2.3 Parametrization

The parameters in the submodels for the mass flow and efficiency are calculated by solving a non-linear least squares problem, formulated as

$$\min V(\theta) \quad (6.11)$$

where  $V(\theta)$  is the cost function

$$V(\theta) = \frac{1}{K} \sum_{k=1}^K (y_k^{mod} - y_k^{meas})^2 \quad (6.12)$$

The parameters  $\theta$  in the model are optimized by minimizing the sum of the difference between measured output  $y_k^{meas}$  and output from the model  $y_k^{mod}$ . The turbine mass flow is taken from engine measurements, the turbine efficiency for each stationary working point is calculated from a turbine map similar to the one in figure 5.1.

### 6.2.4 Validation

The complete turbine model is simulated with data from engine test cell. In this validation, the stationary points with turbine speeds below 20000 rpm are removed since low turbine speeds are hard to measure accurately. The result can be seen in figure 6.1. Noteworthy is that the turbine efficiency is not validated in this figure. Instead, the temperature after the turbine that is calculated as a function of the turbine efficiency is shown. From this figure, it is obvious that the mass flow model has been improved, compared to figure 4.22 on page 31. The correct mass flow is achieved for all stationary working points. The temperature after the turbine is calculated in the same way for this model and the existing turbine model. Therefore there is no noticeable difference between this figure and figure 4.22. The model is implemented in Matlab Simulink, the result can be seen in figure 6.2.

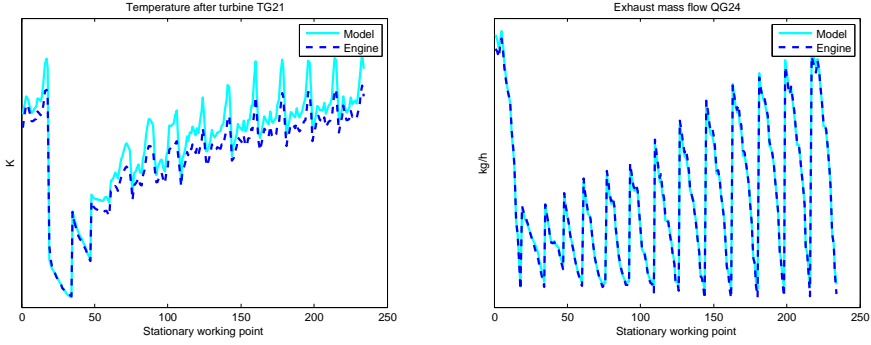


**Figure 6.1.** Temperature after turbine and turbine mass flow when the new model is simulated with data from engine test cell. The turbine mass flow shows a much better fit to engine data than the previous turbine model.

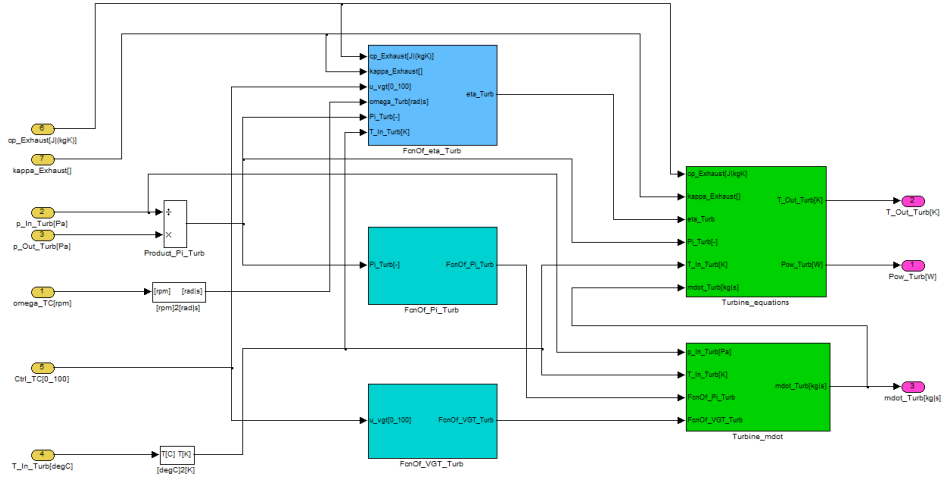


**Figure 6.2.** Turbine model implemented in Matlab Simulink. The block `FcnOf_eta_Turb` calculates the turbine efficiency  $\eta_t$ . The temperature after the turbine  $T_t$  and the turbine power  $P_t$  are calculated in the block `Turbine_equations`. `FcnOf_Pi_Turb`, `FcnOf_VGT_Turb` and `Turbine_mdot` are used to calculate the turbine mass flow  $W_t$ .



# Chapter 7

## Future work

In this chapter, the work that should be done to further increase the confidence of the automated EMS testing is presented.

### **Turbine model**

The turbine model, developed in chapter 6, should be used in the engine model instead of the current turbine model. The new turbine model shows a much better fit to engine test cell data than the old model, this is shown in figure 6.1 on page 43.

### **Compressor model**

As seen in section 4.2.3 and 4.2.4, the existing compressor model that calculates the pressure after the compressor shows a bad fit to engine test cell data. This model is one of the reasons to the high pressures in the HIL simulator. In this model, the pressure after the compressor is calculated as a product of the pressure before the compressor and the compressor pressure ratio, according to equation 5.14 on page 38. The compressor ratio  $\Pi_c$  is derived from a compressor map, shown in figure 5.1 on page 36. The validity of this map should be investigated, since it causes incorrect pressure values after the compressor.

### **Crankshaft torque**

In the existing engine model, the relation between injected fuel and crankshaft torque is poorly modeled. The same amount of injected fuel at the same engine speed results in a too high crankshaft torque in the HIL simulator. This can be seen in figure 4.8 on page 22 and figure C.1 on page 59. This behaviour should definitely be corrected in order to get the same torque output from the model and the real engine.

### **Aftertreatment system**

In the HIL simulator at Scania CV, the control unit for the aftertreatment system EEC is also being tested. The measurements on the  $NO_x$  levels before and after the SCR catalyst shows a very bad fit to engine test cell data, shown in figure B.7 on page 58. To achieve reliable results from the automated EEC testing, the model of the exhaust system on page 54 needs to be improved. This model includes a submodel for the  $NO_x$  emissions.

### **Validate other engine models**

The automated validation method developed in this thesis is also applicable to other engine models in the HIL simulator. In the future, these models should also be validated against engine test cell data.

# Chapter 8

## Summary and conclusions

### 8.1 Summary

The validation method, implemented in Python, makes the comparison between model data and recordings from engine test cell reliable. Both static and dynamic validation have been performed, to be able to study the complete behaviour of the engine model. The validation has identified the torque, turbocharger and aftertreatment models as the weak parts of the current engine model. One part of the turbocharger, i.e. the turbine model, has been improved by creating semi-physical models of the turbine efficiency and the turbine mass flow.

Simulations of the new turbine model shows a good fit to engine test cell data. The current turbine model should definitely be replaced by this model, to increase the confidence of the automated EMS testing at Scania CV. In the future, the compressor, combustion and aftertreatment models should also be improved.

### 8.2 Conclusions

The validation of an engine model in a HIL simulator is a lot more complicated than model validation in general. This is due to the fact that the model inputs and outputs are connected to the engine control unit. The inputs to the model are thereby very hard to control, which makes it difficult to perform a trustworthy comparison.

The validation method developed in this thesis, with the aim to control different model variables in separate threads in a Python script, works well for static as well as dynamic validation. This validation method should definitely be used to validate engine models at Scania CV in the future.





# Bibliography

- [1] Jean Brunet, Luc Flambard, and Atilla Yazman. A hardware in the loop (HIL) model development and implementation methodology and support tools for testing and validating car engine electronic control unit (ECU). 2005.
- [2] Alain Chevalier, Martin Müller, and Elbert Hendricks. On the validity of mean value engine models during transient operation. *SAE Technical Paper*, 2000-01-1261, 1, 2000.
- [3] dSpace GmbH. *Scania Pt Software Documentation version 1.0*, 2006.
- [4] Wang Enhua, Xia Shengzhi, Shi Wei, Li Kang, Chen Yanchun, and Zhang Jianrui. Real-time modeling and simulation of a heavy duty diesel engine. *IEEE Vehicle Power and Propulsion Conference (VPPC)*, 2007.
- [5] Lars Eriksson. Mean value models for exhaust system temperatures. *SAE 2002 Transactions, Journal of Engines*, 2002-01-0374, 111(3), September 2003.
- [6] Lars Eriksson. Modeling and control of turbocharged SI and DI engines. *Oil & Gas Science and Technology - Rev. IFP*, 62(4):523–538, 2007.
- [7] Lars Eriksson and Lars Nielsen. *Modeling and Control of Engines and Drivelines*, 2009. Course material.
- [8] Lars Eriksson, Lars Nielsen, Jan Brugård, Johan Bergström, Fredrik Pettersson, and Per Andersson. Modeling of a turbocharged SI engine. *Annual Reviews in Control*, 26(1):129–137, October 2002.
- [9] Lars Eriksson, Johan Wahlström, and Markus Klein. *Physical Modeling of Turbocharged Engines and Parameter Identification*, pages 59–79. Springer Verlag, 2009. In: *Automotive Model Predictive Control: Models, Methods and Applications*, Editors: L. del Re, F. Allgöwer, L. Glielmo, C. Guardiola, and I. Kolmanovsky.
- [10] Torkel Glad and Lennart Ljung. *Reglerteknik - Grundläggande teori*. Studentlitteratur, Fourth edition, 2006.
- [11] Lino Guzzella and Christopher Onder. *Introduction to Modeling and Control of Internal Combustion Engine Systems*. Springer Verlag, First edition, 2004.

- [12] R. Isermann, J. Schaffnit, and S. Sinsel. Hardware-in-the-loop simulation for the design and testing of engine control systems. *Control Engineering Practice*, 7:643–653, 1999.
- [13] Xu Jie, Wu Feng, Yao Dongwei, Zhang Yongguang, and Guo Qiang. An application of real-time engine model in HILS simulation and testing platform based on SIMULINK. In *Digital Manufacturing and Automation (ICDMA)*, volume 1, pages 176–180, ChangSha, 2010.
- [14] S.J. Lee, K. Park, T.H. Hwang, J.H. Whang, Y.C.Jung, and Y.J. Kim. Development of hardware-in-the-loop simulation system as a testbench for ESP unit. *International journal of Automotive Technology*, 8:127–259, 2007.
- [15] Johan Wahlström. Modeling of a diesel engine with intake throttle, vgt and egr. Technical report, Vehicular systems, 2010.
- [16] Johan Wahlström and Lars Eriksson. Modeling diesel engines with a variable-geometry turbocharger and exhaust gas recirculation by optimization of model parameters for capturing non-linear system dynamics. *Proceedings of the Institution of Mechanical Engineers, Part D, Journal of Automobile Engineering*, 225(7):960–986, 2011.

# Appendix A

## Simulink models below the top layer

The top layer of the engine model is shown in figure 1.1 on page 2. Figure A.1-A.5 shows the content of the Simulink blocks FuelSystem, PistonEngine, AirPath, ExhaustSystem and CoolingSystem. Detailed information about these blocks can be found in section 3.2.2 on page 11.

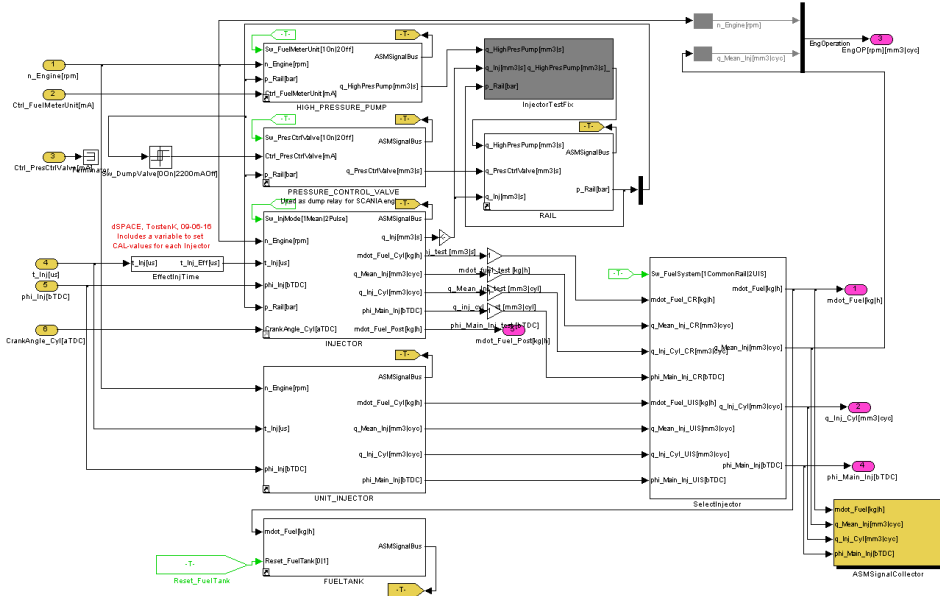
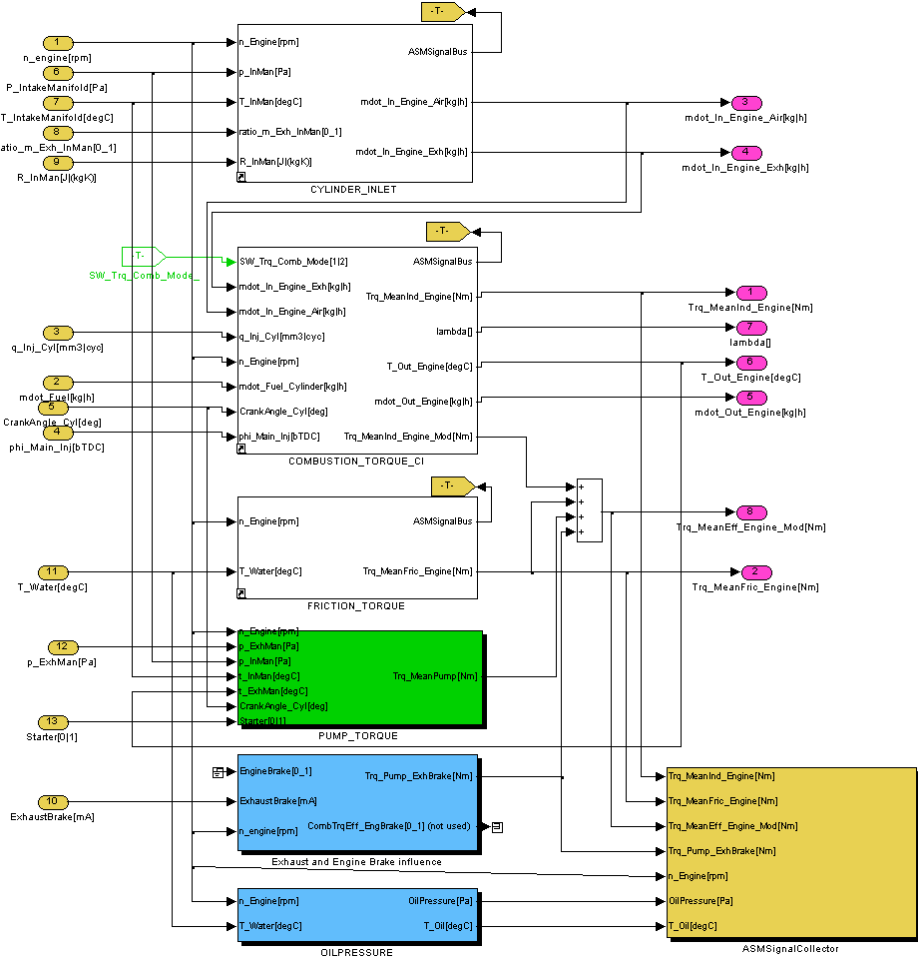


Figure A.1. FuelSystem.

Figure A.2. *PistonEngine*.

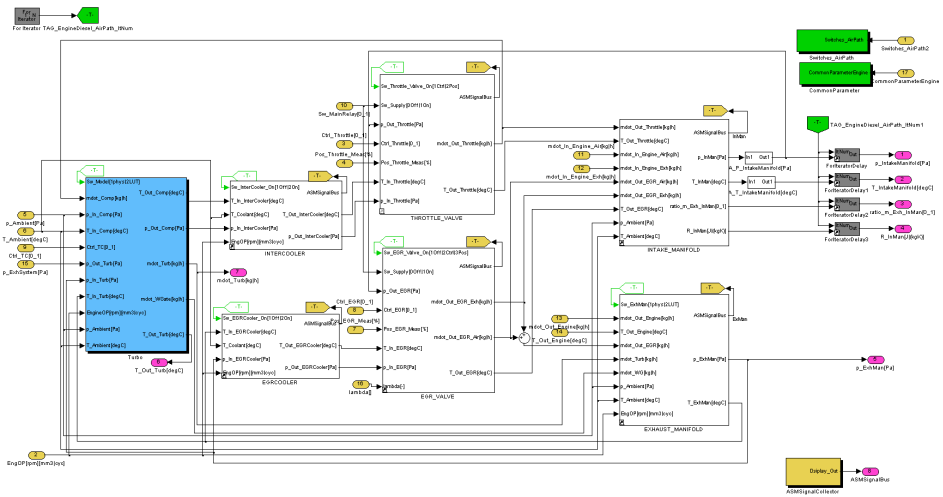


Figure A.3. AirPath.

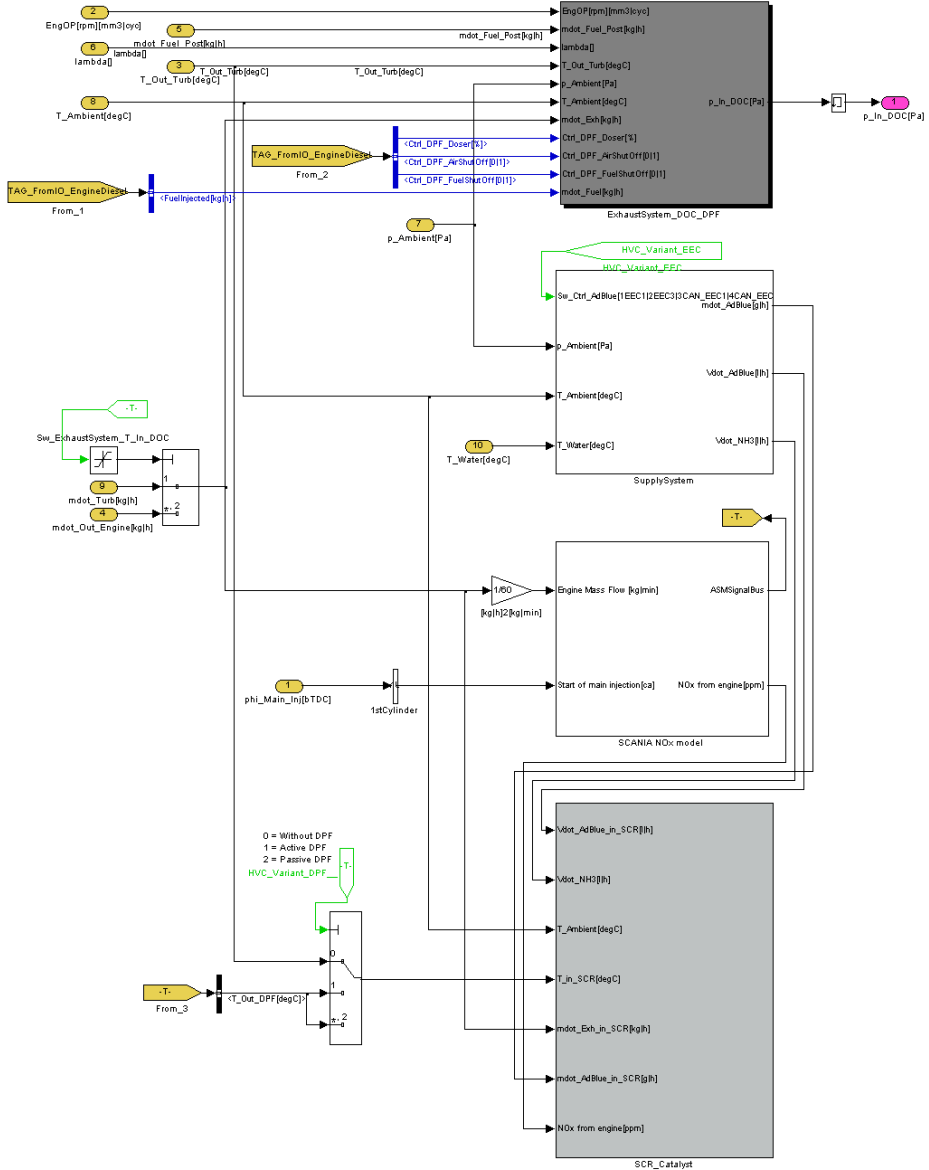
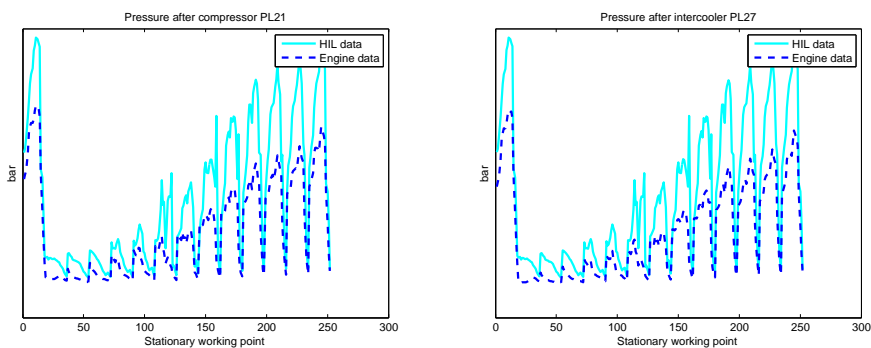


Figure A.4. ExhaustSystem.

**Figure A.5.** *CoolingSystem.*

## Appendix B

# Figures from static validation with VGT and EGR control



**Figure B.1.** Pressure before and after intercooler, high pressures in the HIL simulator for the high load working points.



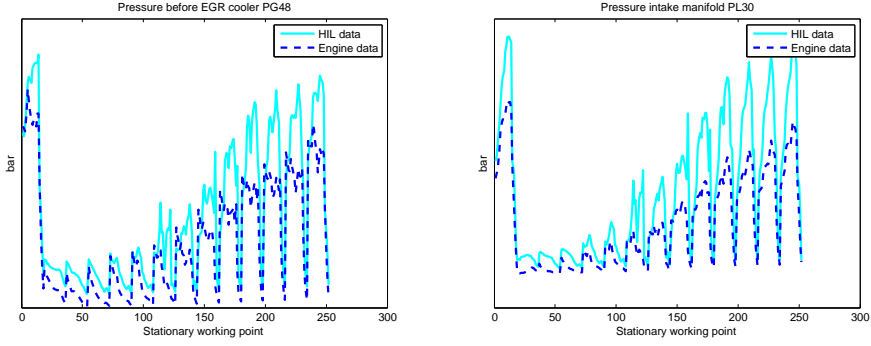


**Figure B.2.** Pressure before and after EGR cooler, high pressures in the HIL simulator for the high load working points.

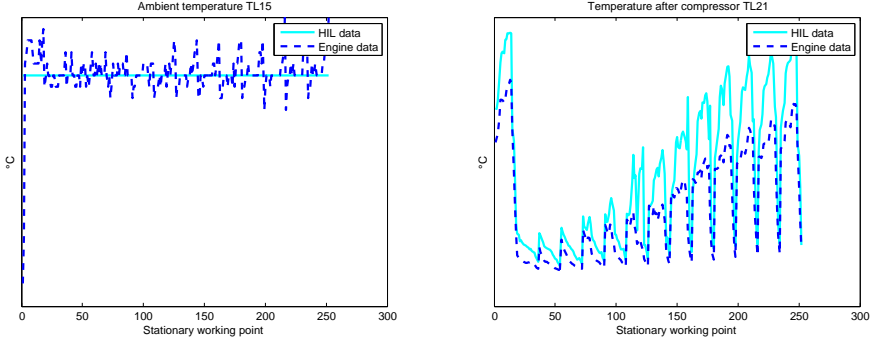


**Figure B.3.** Temperature before and after compressor. The high temperature after the compressor in the HIL simulator is a consequence of the large mass flow through the compressor.

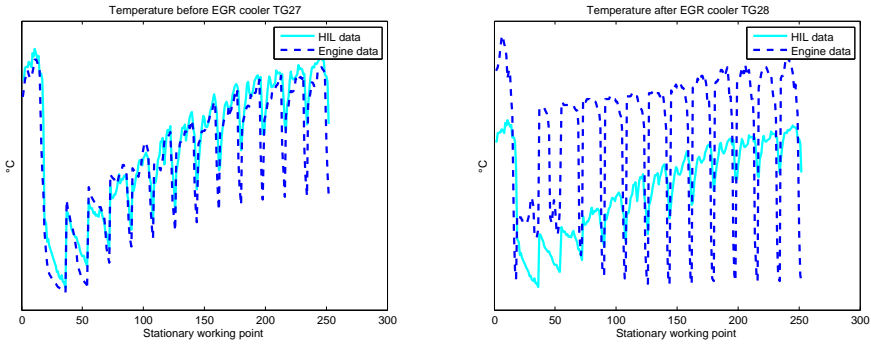


**Figure B.4.** Temperature before and after EGR cooler. The temperature after the EGR cooler seems to be modeled incorrectly in the HIL simulator.

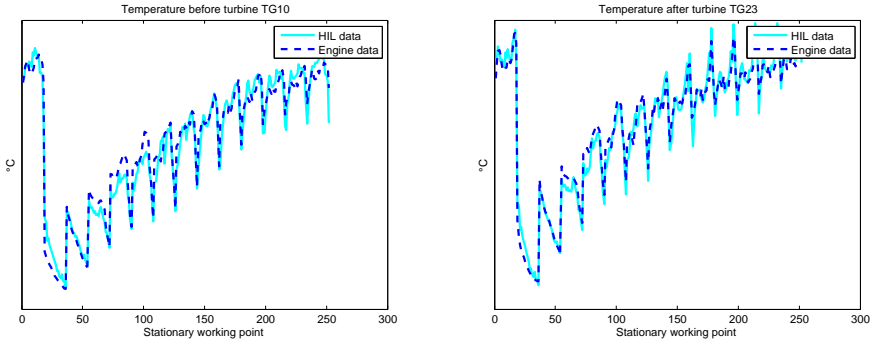


**Figure B.5.** Temperature before and after turbine, both show a good fit to engine test cell data.

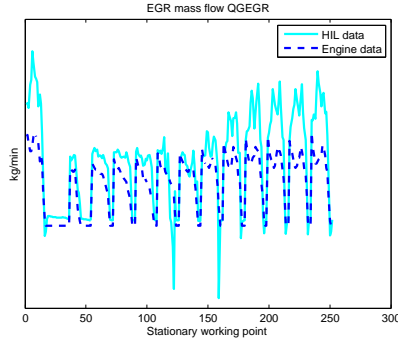


**Figure B.6.** EGR flow. For the high load points, this value is nearly two times larger in the HIL simulator. The control of EGR positions result in a negative EGR flow in some working points. When the pressure is higher in the inlet than in the outlet of the engine, the EGR valve should normally be closed.

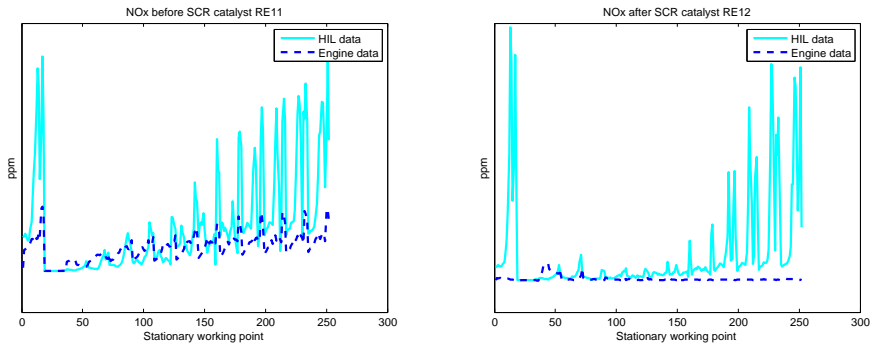


**Figure B.7.**  $\text{NO}_x$  before and after SCR catalyst. The  $\text{NO}_x$  levels before the catalyst is higher for the HIL simulator. Furthermore, the  $\text{NO}_x$  levels are much more reduced in the SCR catalyst for the real engine.

## Appendix C

# Figures from static validation with control of compressor flow and EGR position

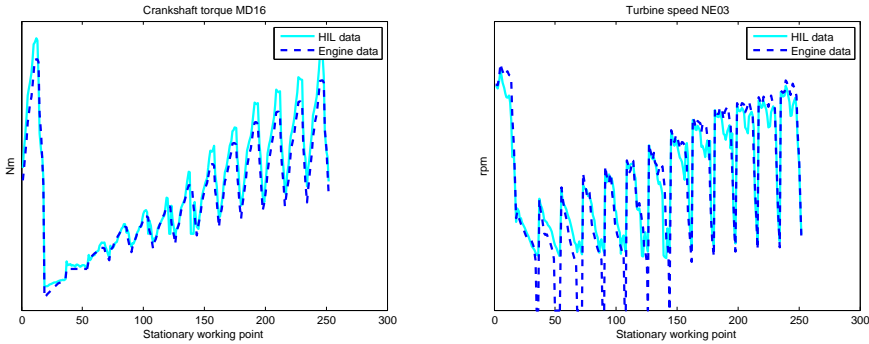


**Figure C.1.** Crankshaft torque and turbine speed (values less than 20000 rpm are recorded as 0 in the engine test cell data). The crankshaft torque is larger in the working points where the correct amount of fuel is reached. The turbine speed shows a good fit in the working points where the correct compressor flow is achieved.

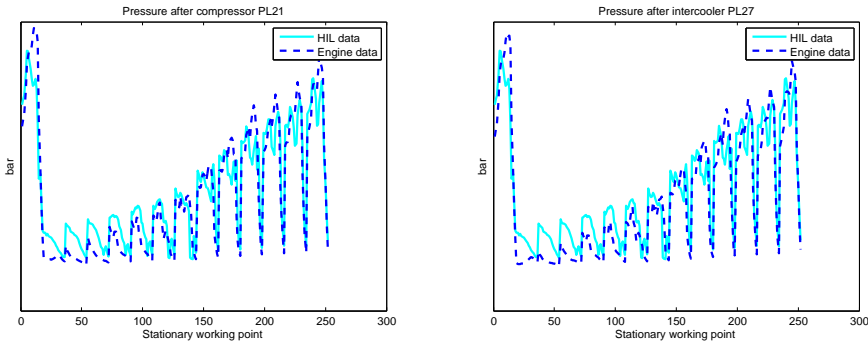


**Figure C.2.** Pressure before and after intercooler. These pressures show a good fit in the high load working points with the same mass flow in HIL simulator and engine test cell. For the low load points, the correct mass flow is not achieved and hence the pressures are too high in the HIL simulator.

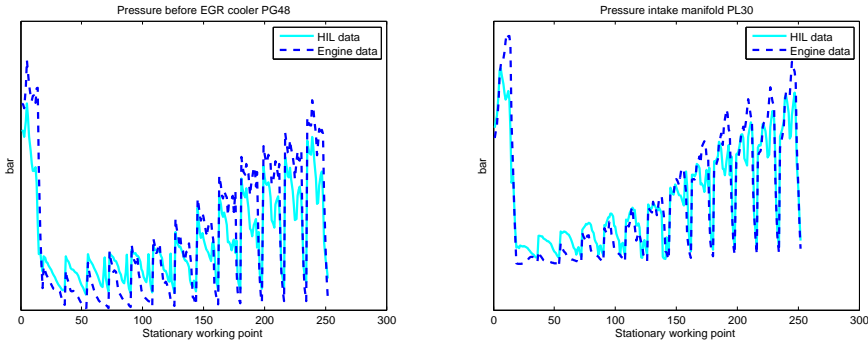


**Figure C.3.** Pressure before and after EGR cooler. Shows a good fit where the correct mass flow is achieved.

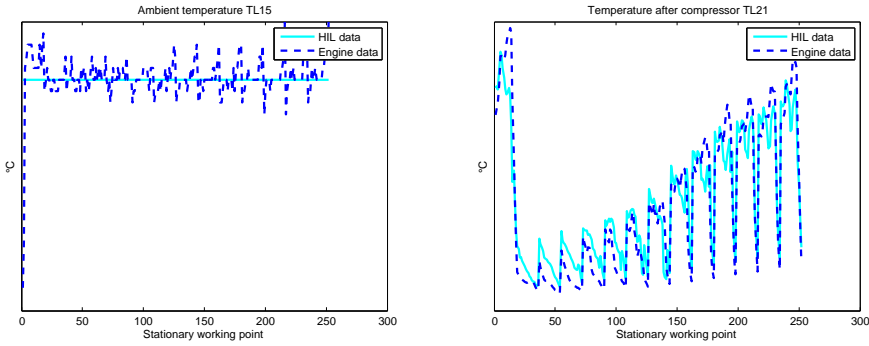


**Figure C.4.** Temperature before and after compressor. Compared to figure B.3, the temperature after the compressor in the HIL simulator shows a much better fit to engine test cell data when the correct mass flow is achieved. Consequently, a large mass flow through the compressor will lead to a high temperature after the compressor.

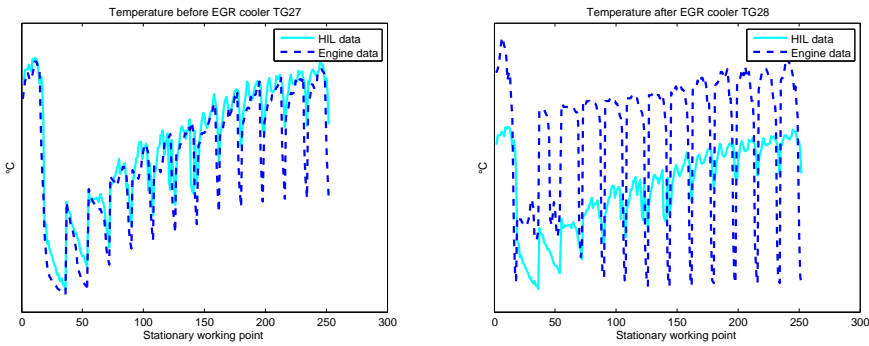


**Figure C.5.** Temperature before and after EGR cooler. The EGR cooler efficiency seems to be modeled incorrectly.

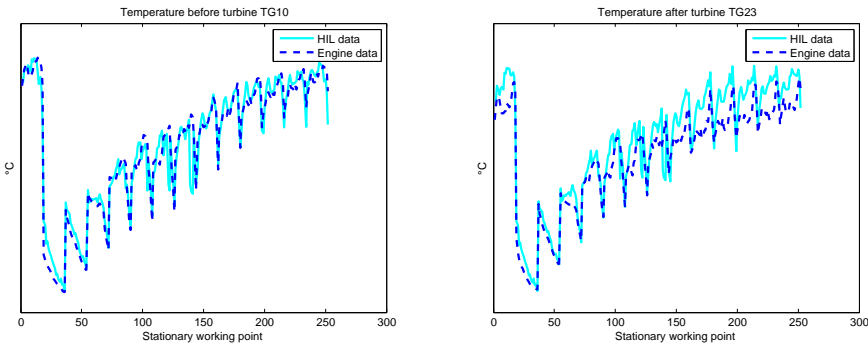


**Figure C.6.** Temperature before and after turbine. These temperatures show a good fit to data from engine test cell, except from a small difference in the temperature after the turbine.

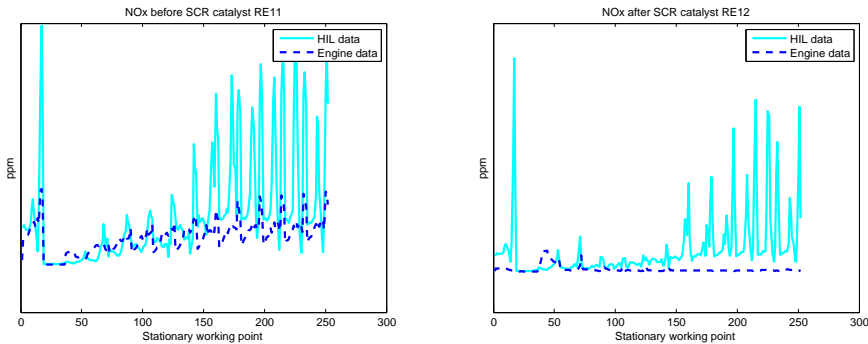


**Figure C.7.** NOx before and after SCR catalyst. These figures show that the  $NO_x$  model, shown in figure A.4 on page 54, needs to be improved.

## Appendix D

# Figures from dynamic validation

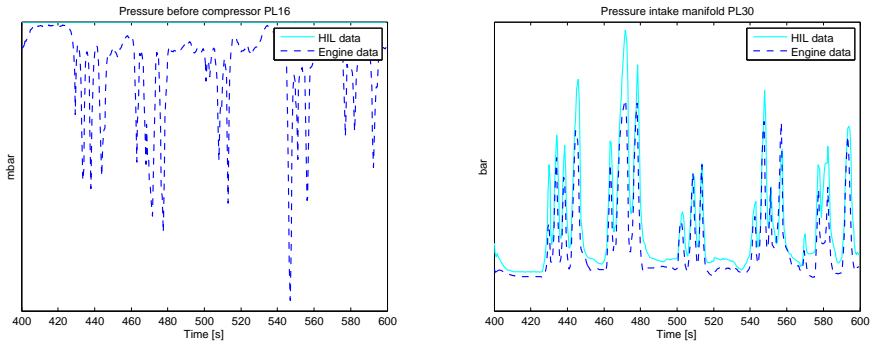


**Figure D.1.** Pressure before compressor and pressure in intake manifold. Analogically to the steady state validation, the pressure in the intake manifold is too high in the HIL simulator.

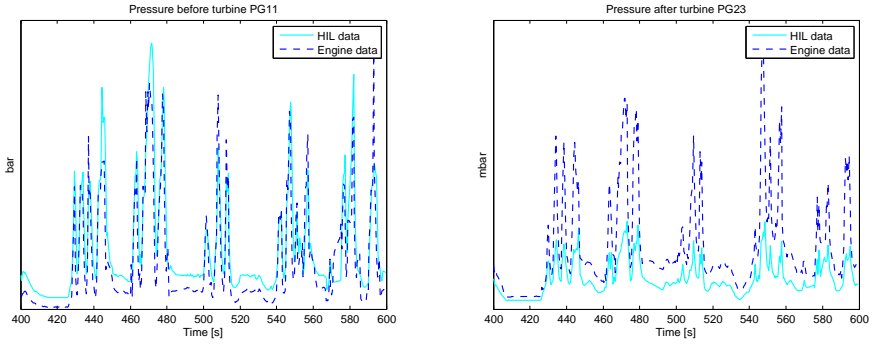


**Figure D.2.** Pressure before and after turbine. This figures show the same results as in the steady state validation. The pressure before the turbine is too high and the pressure after the turbine is too low in the HIL simulator.

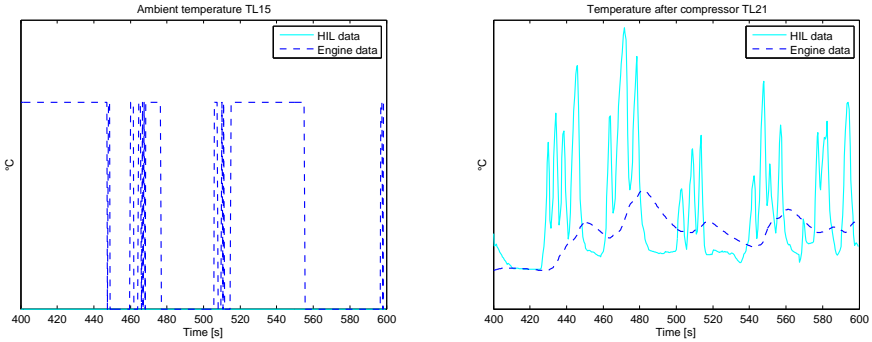


**Figure D.3.** Temperature before and after compressor. The right figure shows faster temperature dynamics in the HIL simulator than in the engine test cell. The time constant of the temperature sensor in the engine test cell can be the source to this deviation.

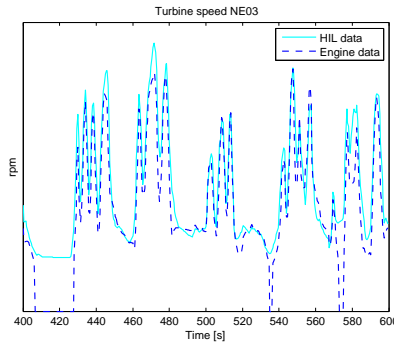


**Figure D.4.** Turbine speed (values less than 20000 rpm are recorded as 0 in the engine test cell data). The turbine speed is too high in the HIL simulator. This behaviour is also seen in the steady state validation.